LASER-ASSISTED SECONDARY ION MASS SPECTROSCOPY AND ITS APPLICATIONS IN PRACTICAL SURFACE ANALYSIS

by

Mehmet Cem Karahan

A thesis submitted in partial fulfillment of the

requirements for the degree of

Master of Science

in

Electrical Engineering

Montana State University
Bozeman, Montana
July, 2004

APPPOVAL

of a thesis submitted by

Mehmet Cem Karahan

This thesis has been read by each member of the thesis committee and has been found to be satisfactory regarding content, English usage, format, citation, bibliographic style, and consistency, and is ready for submission to the college of Graduate Studies.

Dr. David Dickensheets

Approved for the Department of Electrical & Computer Engineering

Dr. James Peterson

Approved for the College of Graduate Studies

Dr. Bruce McLeod

STATEMENT OF PERMISSION OF USE

Mehmet Cem Karahan

July 19, 2004

DEDICATED TO

MY PARENTS

KUTLU AND ASUMAN KARAHAN

AND

MY SISTER

ZEYNEP KARAHAN

ACKNOWLEDGEMENTS

The successful completion of this project required the help and advice of many people. Their valuable input helped me stay the course to finish the most challenging project of my life. I would like to thank all those who contributed.

First and foremost, I owe my advisor, Dr. Recep Avcı, a debt of gratitude. Without his guidance and never-ending support this project never could have been finished. He was always available for teaching and supporting me on all aspects of this research. I appreciate greatly, all of his help from the start of this project, all the way to the final editing of this thesis.

I would like to thank Nancy Equall, who not only provided my initial training in ToF-SIMS, but was always available whenever I had questions or was in need of advice.

Next, I would like to thank all those who have made a significant contribution to the completion of this work: Dr. Jan Sunner for helping me understand more about mass spectroscopy and providing samples to be tested by the new platform, Dr.David Mogk for preparing substrates associated with the Oxygen exchange experiments included in this thesis, Dr. Şenay Yalçin for staying many nights with me in the lab to complete these experiments and Dr. Gary Groenewold for his various contributions in this thesis. I also thank Dr. Jahson Suozy for providing MALDI samples that helped me verify the operation of the new platform.

I would like to thank Dr. David Dickensheets and Dr. Shaw for their advice and for serving as members of my graduate committee.

Thirdly, I would like to thank the past and present ICAL staff who put up with me in the past two years: Dr. Jim Anderson, Dr. Fernando Teran Arce, Dr. Robert Boyd, Pat Gale, Brett Fors, Tiffany Kniepkamp, Bo Glaspey, Angie Cheff, Kendra Krantz, Tanner Horne, Melody Bergeron, Megan Arthun, Kelly Cole, Kadia Schuneman.

I would like to thank my parents Kutlu and Asuman Karahan and my sister Zeynep for providing the most supportive and warmest family environment, and always being there when I need them. Without them, I would not be where I am today. I would also like to thank my girlfriend Collette Campion, who always believes in me and never stops supporting me.

Finally, and most importantly, I thank God. My faith and God's blessing helped me complete this project and always give me the strength I need.

TABLE OF CONTENTS

TABLE OF CONTENTS - CONTINUED

LIST OF TABLES

LIST OF FIGURES

LIST OF FIGURES - CONTINUED

Figure Page

LIST OF FIGURES - CONTINUED

Figure Page

ABSTRACT

This thesis presents the development and the implementation of a combined practical surface analysis platform. The combined system incorporates a Laser Desorption (and Ablation) Mass Spectroscopy (LDMS) system into a Time-of-Flight Secondary Ion Mass Spectroscopy (ToF-SIMS) instrument under a single virtual control platform. This is accomplished via customized instrumentation control as well as data acquisition and analysis routines all implemented on the LabVIEW programming environment. The system is named *Laser-Assisted Secondary Ion Mass Spectroscopy* (LASIMS). The system has the flexibility of carrying out surface characterization and chemical imaging experiments utilizing both the ToF-SIMS and LDMS techniques, generating complementary information from the *same area* of the sample at (nearly) the *same time*. A subclass of LDMS is the powerful Matrix-Assisted Laser Desorption/Ionization (MALDI) spectroscopy technique, which now is used routinely in this system. The combined system offers many other practical uses and applications such as laser cleaning of thin metallic films coating an insulating sample to carry out rapid ToF-SIMS analysis of such samples, as well as laser-induced enhancement of secondary ion detection of radionuclides, such as ^{137}Cs and U, and the study of isotopic Oxygen exchange on reactive oxide mineral surfaces, which are all detailed in the thesis. We have also tested the fundamental question of whether or not laser and particle beam excitations couple during the desorption and ionization process. The test basically utilizes a short (few ns) laser pulse to bring the surface of the sample to just under laser desorption/ionization threshold by means of local heating and/or photochemical processes, while a focused Ga^+ beam that is well synchronized (temporally and spatially) with the laser pulse is used to further energize the sample surface (LASIM excitation) to yield *additional molecular fragments* from that surface. We observed *no* additional fragments as a result of LASIM excitation, suggesting no coupling between particle and laser desorption/ionization mechanisms.

CHAPTER ONE

INTRODUCTION

Surface Analysis

Surface Analysis can be defined as the characterization of the surface region of a sample. Depending on the analysis technique used, this characterization may provide insight about the elemental and/or chemical composition, morphological features, chemical inhomogeneities, or a combination of the above properties about the specimen under investigation [1]. Such information finds applications in academic research as well as in a broad range of industries. For example, semiconductor device fabrication processes depend strongly on surface analytical tools to monitor interface properties, contamination, trace impurities, and monitor reactions on semiconductor wafers. Geologists employ such tools to make isotope measurements in geological samples. The applications are vast and broad.

Types of Surface Analytical Instruments

The range of techniques available today in surface analysis is nearly as broad as its applications. These techniques include electron spectroscopy methods, such as X-ray Photoelectron Spectroscopy (XPS) and Auger Electron Spectroscopy (AES). Electron spectroscopy techniques are considered as the

most mature of surface analytical tools. More recent techniques include X Atomic Force Microscopy (AFM), Secondary Ion Mass Spectroscopy (SIMS). These techniques are often surface and application specific. Of these numerous techniques, SIMS is the most surface-sensitive technique allowing, chemical mapping with sub-micron resolution. It also has the capability of detecting trace elements, even though it still lacks the quantitative analysis possible with Auger and XPS.

SIMS

A Brief introduction to Mass Spectroscopy

Secondary Ion Mass Spectroscopy is based on the fact that charged and neutral secondary species are emitted (sputtered) from a sample surface that is subjected to energetic primary particle bombardment. The secondary species can take many forms: Electrons, neutral atoms and molecules, and most importantly, atomic and molecular ions [2]. Mass spectrometers selectively detect these secondary ions to produce a mass spectrum characteristic of the specific chemical structure of a surface.

Over the years, various models attempting to describe the process leading to the sputtering of secondary species from a sample surface have been put forth, with only one prevailing and still widely accepted today. The collision cascade model, developed by P. Sigmund, has had the most success in explaining the naturally observed phenomenon associated with typical SIMS experiments [3]. In this theory, it is supposed that the energy of the primary

particles is transferred to the atoms making up the surface region of a solid sample by the collisions taking place during the primary beam bombardment. This energy transfer leads to a series (cascade) of collisions within the solid. Of this cascade of collisions, some return to the surface, which results in the emission of secondary species. A portion of these emitted species are ionized in the course of the sputtering process. It is these species that can be mass analyzed and detected with the use of a mass spectrometer comprised of ion extraction and ion transfer lenses. The collision cascade model is illustrated in Figure 1.1.

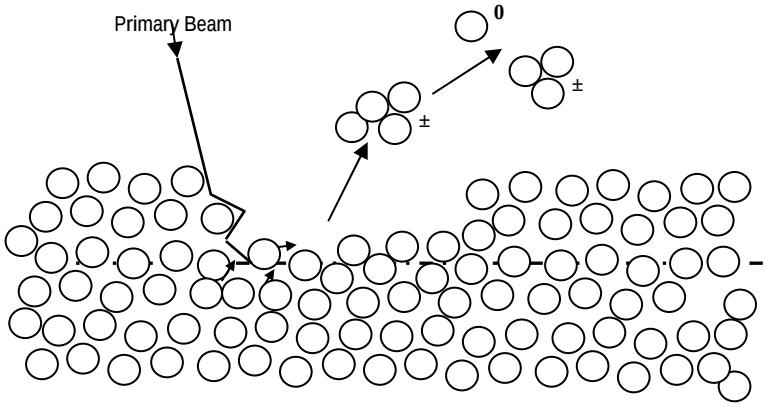

Figure 1.1 The collision cascade model and the emission of the secondary species [2].

Although the specific designs of mass spectrometers vary, in general all of these instruments possess the same building blocks. Typical components are illustrated below in Figure 1.2.

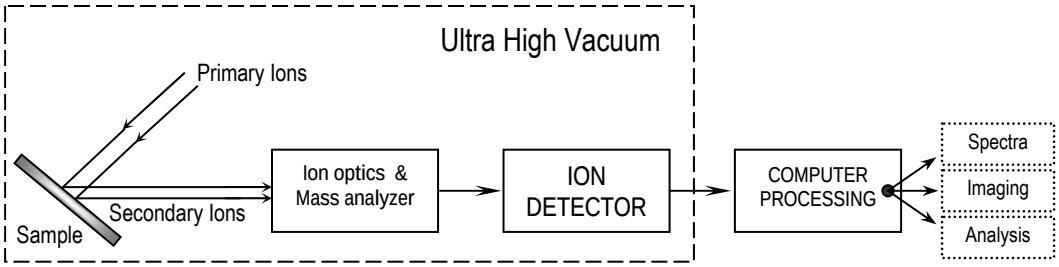

Figure 1.2 Typical components of a SIMS instrument.

Mass spectrometers, in addition to possessing a source made up of a focused primary beam of particles need a means of separating the secondary species emitted from the surface of the sample in question. This separation is organized as the mass-to-charge (m/z) ratio of the ions entering the mass analyzer. Many different types of mass analyzers can be employed for mass separation. Earlier instruments utilized *magnetic sector field* analyzers. *Double-focusing sector field* analyzers and *quadrupole* instruments have also been applied successfully. High-performance imaging SIMS instruments employ *time-of-flight* type analyzers. This type of analyzer is capable of delivering nearly 100% efficiency, as well as maximum mass range of detection for the secondary ions generated as a result of primary ion impact.

The need for the avoidance of surface contamination and collisions between gas molecules and the secondary species under analysis require the mass analyzer and ion detection units to be under ultra high vacuum (UHV) conditions. In fact, advances in vacuum technology greatly benefited the development and implementation of modern mass spectrometer designs.

Time of Flight (TOF) – SIMS

The design of Time-of-Flight type mass analyzers are based on the fact that the flight times of the emitted secondary ions along the flight path in an UHV environment can be directly related to the mass-to-charge ratio (m/z) of the secondary ions. Considering two ions of the same charge and different masses,

the heavier ion should take a longer time to complete the flight path as opposed to a lighter ion. This type of instrument generally employs only an electric field to separate ions of different m/z ratios. The behavior of the surface-emitted secondary ions as they make their way through the mass spectrometer is easily explainable with basic Newtonian equations as described in what follows [3].

Before the secondary ions are transferred to the flight path they have to be extracted and accelerated to a predetermined nominal speed. This is achieved in a parallel plate capacitor as part of the extraction optics. The extraction plate of this capacitor is grounded, while the other plate, the sample, is connected to a high voltage supply typically at approximately 3 kV. This scheme is illustrated in Figure 1.3.

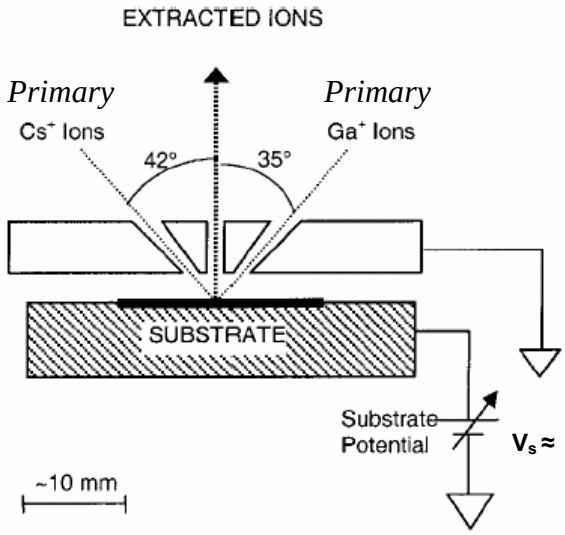

Figure 1.3 TRIple Focus Time of flight (TRIFT) extraction

The effects of the small apertures for the charged particles to enter or exit are neglected in this analysis. Application of a high voltage to the sample generates a uniform electric field in the extraction region, consisting of two parallel-plate capacitors separated by approximately 3 mm. In the presence of an

electric field **E** at a given point in space, the force acting on a secondary ion with charge *z* (typically, z=±q (Charge, Coulomb)) is given by

$$\vec{F} = z \cdot \vec{E} \tag{1.1}$$

Considering the plane-mirror capacitor and uniform electric fields, the scalar version of this equation combined with Newton's 2nd law may be used to describe the acceleration, *a*, experienced by the secondary ions due to the applied electric field.

$$F = z \cdot E = m \cdot a \tag{1.2}$$

The magnitude of the acceleration is given by:

$$a = \frac{z \cdot E}{m} \tag{1.3}$$

Kinematic equations relating the velocity and the displacement of the moving ion under the influence of the uniform electric field in one-dimensional space (such as the extraction region in our ToF-SIMS system illustrated in Figure 1.3) can be found readily by relating the first derivative of velocity, *u*, to the acceleration $a = du/dt$, and the first derivative of displacement, *s*, to the instantaneous velocity, $u = ds/dt$. Integration of these equations with respect to time immediately yields the well-known kinematic equations:

$$u = u_0 + \frac{z \cdot E}{m} \cdot t \tag{1.4}$$

$$s = (u_0) \cdot t + \left(\frac{z \cdot E}{2 \cdot m}\right) \cdot t^2 \tag{1.5}$$

where the initial values for the axial velocity component and the displacement at time *t=0* are assumed to be $u=u_0$ and *s=0*, respectively. The *s=0* corresponds to

the sample surface, while the *t=0* corresponds to the time the primary ion pulse hits the surface. The initial velocity u_0 corresponds to the axial component (perpendicular to the surface) of the velocity imparted on the secondary ions due to secondary ion emission process, and is typically a very small fraction of the drift velocity acquired by these ions in the extraction region. From these equations, the time, t_e, spent in the extraction region can be expressed as:

$$t_e \cong \sqrt{\frac{2md}{z\,E}} \tag{1.6}$$

where $d \cong 3$ mm is the separation between the extraction plates.

Secondary ions accelerate due to the energy received from the electric potential acting on them. These species also possess a potential energy, which is equal to the product of their total charge, *z*, and the electric potential V(s) at a distance s:

$$U = z \cdot V(s) \tag{1.7}$$

The total energy of the moving ion is preserved in the electric field: $U + K = const$. Assuming that the ground plate is the reference for the electric potential (i.e. *V=0*) and the kinetic energy of the ions at the sample surface is K_0, the total potential energy of the system is at a maximum at the sample surface and zero at the extraction plate where electric potential is zero.

The strength of the electric field, *E*, can be related to the electric potential, *V*, at the same point via

$$V(s) = E \cdot (d - s) \tag{1.8}$$

where d is the separation between the sample and the grounded extraction plate.

Taking into account the principle of conservation of energy, $U(s)+K(s)=U(0)+K_0$, the total energy of the secondary ions in motion at location *s* can be expressed as:

$$z \cdot V(s)+\frac{1}{2}m \cdot (u_d)^2 = z \cdot V_0 + K_0 \tag{1.9}$$

where V_0 is the electric potential applied to the sample (typically about 3 kV), and K_0 is the initial kinetic energy of the secondary ion as it was desorbed from the surface. In practice $K_0 << qV_0$, that is to say the initial kinetic energy of the secondary ions range from meV to eV, depending on whether or not these ions are molecular or atomic species, respectively. The potential energy of a singly ionized secondary ion is typically about 3 keV. This means K_0 can be ignored as compared to the zV_0 term in the above equation, which by setting *s=d* yields:

$$z \cdot V(d)+\frac{1}{2}m \cdot (u_d)^2 = z \cdot V_0 \tag{1.10}$$

Recalling that *V(d)=0*, this expression yields the velocity of the secondary ion when it reaches the extraction plate. u_d is called the drift velocity, which is the velocity of the secondary ion at the extraction plate. This is the parallel (to the optical axis) component of the secondary ion velocity at the extraction plate given by:

$$u_d = u_0 + \sqrt{\frac{2 \cdot z \cdot V_0}{m}} \cong \sqrt{\frac{2 \cdot z \cdot V_0}{m}} \tag{1.11}$$

Note that the expression for the drift velocity has an unknown axial component u_0 due to the initial velocity of the secondary ions. The principal design aim of all ToF-SIMS instruments is to compensate for this radial component of the initial

velocity so that time of flight of the secondary ions for a given nominal mass would be more or less the same for a given mass. The ability of the system to perform this compensation relates directly to the most crucial element of the instrument performance, mass resolving power. Mass resolution in a TOF-SIMS instrument refers to the ability of the system to separate ions of comparable m/z, and it is measured as the ratio, $m/\Delta m$, where m represents the mass of the secondary ion and Δm is the full width at half maximum of the peak. Without this compensation the resolution of the instrument would suffer greatly.

However, as mentioned above the parallel and perpendicular (radial) components of initial velocity are unknown and even though in the calculations we have ignored these unknown components, the ion optics in the transfer and the drift region cause those secondaries deviating from the ideal velocities to follow longer trajectories hence compensating for their excess speed and direction as shown in Fig. 1.4. In this way, all the secondary ions with the same nominal mass arrive at the detector within a short period of each other, allowing excellent mass resolution (up to 10,000 at 42 amu). The ion trajectory compensation mechanism for the SIMS instrument for this rese

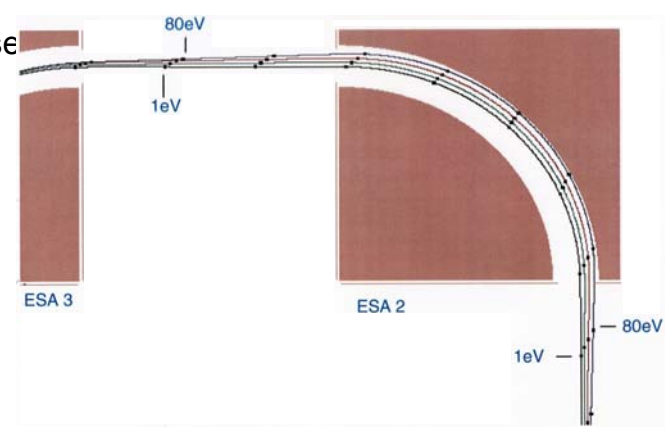

Figure 1.4 Flight paths for ions of different initial energy but same nominal mass in the TRIFT spectrometer.

The time of flight in the drift region, t_D, of the ions can then be determined by

$$t_D = \frac{D}{u_D}$$

or

$$t_D = \frac{D}{u_d} = \frac{D}{u_0 + \sqrt{\frac{2 \cdot zV_0}{m}}} \cong D\sqrt{\frac{m}{2 \cdot zV_0}} \qquad (1.12)$$

The total time of flight (TOF) experienced by the secondary ions is the sum of the times spent in various regions, such as time spent in the accelerating region (t_a) in addition to transfer regions, and the time spent in the drift region (t_D).

$$TOF = t_a + t_D$$

Considering that $u_0 << u_d$ the TOF can be expressed in terms of mass, m of the secondary ion simply by

$$TOF \cong t_a + D\sqrt{\frac{m}{2zV_0}} \qquad (1.13)$$

For mass calibration purposes the relationship between the measurable quantity TOF and the mass m of the secondary ion can be written as

$$\sqrt{m} = a \cdot TOF + b \qquad (1.14)$$

where *a* and *b* are determined empirically in a typical calibration procedure. Such a mass calibration involves typically three data points comprised of three well-separated secondary ion masses and their measured TOFs. Once *b and a* are determined the relation above appears to work for large range of mass

determinations, from zero to tens of thousands of amu. The mass calibration described above is independent of primary ion source. The same procedure is used for mass calibration regardless of whether a primary focused ion beam or pulsed laser beam is used as the excitation source.

Other ToF related techniques in Mass Spectrometry

Laser Desorption Mass Spectroscopy (LDMS)

This method of mass spectrometry makes use of a laser source, typically in the wavelength ranges of UV to IR, as a primary beam to produce secondary ions from an irradiated sample surface. The laser source is operated in a pulsed mode, making LDMS a compatible technique to employ with TOF-SIMS hardware. The laser has the function of not only desorbing species from the sample, but also to ionize these secondaries [2]. The desorption process takes place when the energy provided via the laser irradiation exceeds a certain threshold value [3]. At low laser fluences (energy /area), the laser desorption spectra can be complementary to that of SIMS obtained by ion bombardment. There is no single model that has been successful in describing the observed ionization behavior of secondary species upon laser irradiation. The most agreed-upon model assumes this process is based on photochemical processes [Selby, 20]. A distinctive advantage of LDMS seems to be its versatility observed in its ionization behavior. This follows from observations that the ionization mechanisms associated with LDMS are altered by simply tuning the power

density of the focused laser spot on the sample [4]. The LDMS technique has been applied successfully in order to generate mass spectra from a variety of samples. Amongst other families of samples, LDMS has been successfully applied in the analysis of organic samples as well as the surfaces of industrial polymers [3].

Matrix-Assisted Laser Desorption / Ionization (MALDI)

The mass spectroscopy method of MALDI can be described as a variation of LDMS, whereby specific preparation practices are employed to collect large, intact molecular information from a sample. In MALDI, specific matrices are used to disperse the sample of interest, as well as to isolate the molecules making up the analyte. These matrices are selected based on their wavelength absorbing properties. The matrix serves the primary function of absorbing the wavelength of the primary laser source irradiation.

The most important characteristic of MALDI based experiments is the ability of the technique in desorbing high-mass analyte molecules from a sample. The technique has been applied to numerous types of samples. In 1988, Karas and Hillenkamp reported the detection of proteins with molecular masses in excess of 10,000 Da with irradiation provided by a Q-switched quadrupled Nd-YAG laser lasing at 266 nm [5]. A N_2 laser with a wavelength of 337 nm was used by Tanaka to collect molecular ions up to 100,000 Da in weight [3]. In general, depending on the nature of the analyte, different wavelengths are used

to for irradiation purposes, and in turn this requires different matrices capable of absorbing the wavelength used.

Laser-Assisted Secondary Ion Mass Spectroscopy (LASIMS)

The main objective successfully completed in this research is the interfacing of a N_2 laser as another primary excitation source to complement the particle beam source that was already in place prior to this research. The main motivation behind the interfacing of a laser source to the existing hardware lies in the fact that the excitation mechanism of a laser beam is fundamentally different from that of particle beam, but additionally that the two mechanisms complement each other. Having access to two complementary excitation mechanisms in the same system offers a number of advantages over a system with a single source. The advantages of the laser source will be demonstrated with a number of examples presented in this thesis.

One of the main questions this thesis tries to answer is: Are the two (laser - particle) excitation mechanisms totally independent or is there a coupling between the two mechanisms?

Enhanced molecular information from a sample could be generated if energy could be more efficiently distributed on the excited surface. In fact, research has shown that this can be accomplished using polyatomic projectiles such as $Cs(CsI)_n^+$ clusters, SF_5^+, and ReO_4^-. These bombarding projectiles are thought to probe larger zones where the deposited energy is great enough to produce emission of molecular species, but insufficient to atomize the ejected species.

The origin of the secondary ion enhancement resulting from polyatomic projectile impact is thought to be the result of overlapping collision cascades, which randomly form energized areas that meet the energetic threshold required to desorp and ionize secondary ions. Frequently, however, molecular secondary ions sputtered from mineral surfaces are low in abundance and have limited characterization value, even when using polyatomic projectiles. If a more systematic means of energizing the surface could be identified, then molecular species might be routinely generated, resulting in a greatly augmented ability to characterize the *surface chemistry* (as opposed to merely *composition*) at a *microscopic scale*.

Photon excitation of surfaces represents perhaps the easiest means to energize surfaces, and has been used widely with LDMS methods for this exact purpose [6]. Unfortunately, LDMS suffers from the same problem as SIMS: The technique produces a preponderance of atomic secondary ions, yet tends to be destructive relative to the emission of molecular secondary ions emitted from mineral surfaces. This effect can be mitigated somewhat by reducing the power density of the laser pulse; however, the overall secondary ion abundance is dramatically reduced by this action. However, molecular characterizations with LDMS using low-fluence laser pulses have not been investigated thoroughly and prior research shows that a number of secondary ions generated this way might have diagnostic value. It is noteworthy that for the analysis of biochemicals, matrix-assisted laser desorption mass spectrometry (MALDI) is used to overcome this limitation: With MALDI, the wavelength of the

irradiating laser is matched with an absorption band of an organic *matrix* chemical, which results in efficient excitation of the matrix [7]. The biochemicals, which have been previously dissolved in the matrix, are energized as a result of their proximity with the excited matrix molecules.

In this research, selective photoexcitation of surfaces is combined with coincident projectile bombardment. This combination is appropriately called *Laser-Assisted Secondary Ion Mass Spectrometry*, or LASIMS. In LASIMS, a short (~ 4 nanosecond) laser pulse precedes the SIMS primary ion beam pulse (in fact, the two pulses fall on the area of interest almost instantaneously). The main effect of the laser pulse is to heat a large area, >100 μm in diameter. Very limited ion desorption is expected to result from the laser pulse alone, and thus the energy density in the surface will remain just below the desorption threshold. Consequently, a relatively small additional energy input is hypothesized to result in molecular desorption. This will happen if the excitation mechanism of laser and particle beam couple somehow. This additional energy is supplied by means of a focused primary ion beam (Ga^+ or In^+) with a cross section less than 1 μm in diameter. The advantage here is that the emission will be localized to the point of the primary ion beam. Figure 2.5 shows the emission zone and associated energy density vs. distance from the impact point surrounding one of the primary ions ($P^+ = Ga^+$ or In^+) in the beam. The typical distances involved in the figure do not exceed 10-20 nm (r_3<10-20 nm). While extensive surface damage occurs in the immediate vicinity (<2-3 nm) of the primary ion particle [8], the molecular species, in principle, can be emitted further away from the damaged area.

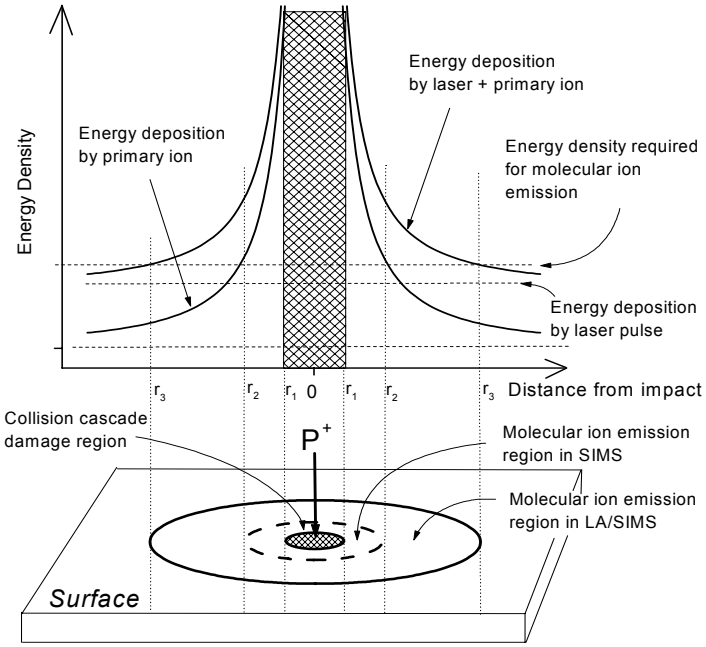

Figure 1.5 The LASIMS idea.

This would allow, just by geometrical considerations, orders of magnitude increase in the yield of the species that can carry chemical information about the material under investigation from a microscopic area. Without the laser assistance, such molecular information from a localized area would not be obtainable. Hence the basic promise of the laser-assisted SIMS is to expand the emission zone from $r_1 < r < r_2$ to $r_2 < r < r_3$, more than an order of magnitude increase in the area from which molecular ions can be emitted.

In the current literature, there is no common consensus on the mechanisms involved in ionization and desorption of molecular species in either SIMS [9] or LDMS [6], though most of the possible governing processes most likely have been considered [6,9]. A synergistic interaction between SIMS and LD surface excitation is, however, predicted in many alternative models [10].

In laser desorption, thermalization of absorbed laser energy plays a major role in the desorption of large molecules. This is supported by the fact that almost identical mass spectra are obtained with IR and UV lasers both in LD and in MALDI [10]. In contrast, molecular emission in SIMS is likely preceded by extensive equilibration of the energy in the keV collision cascade [10, 2], while atomic ions are more directly a result of collision cascade. Whether the localized energy is delivered to the region by a primary ion beam or by a laser beam, molecular fragments will be emitted as long as the total energy density is above the ionization threshold and away from the damage zone. The literature as it stands now does not dispute this assumption [11].

These ideas have been tested in this work. Results of these tests have been included in Chapter 7 of this thesis. We found no experimental evidence supporting the existence of coupling mechanisms between excitation by photons and by energetic ions, even though individually each primary beam is capable of exciting the surface and causing generation of secondary ions.

Thesis Overview

Chapter 2 provides a description of the existing system prior to the start of this project. Subsequently, the modifications put into place to achieve the objectives of this research are offered. Additionally, the software written to provide the instrument control associated with the new system is described.

The remaining chapters offer insight to the applications of the LASIMS platform.

Chapter 3 describes the application of the laser source as a charge compensation tool in the analysis of insulating samples.

Chapter 4 reports the advantages introduced by the laser source in the enhancement of secondary ion yield of toxic-contaminated soil samples.

Chapter 5 contains information about the ‘Isotopic Oxygen Exchange’ experiments carried out as a part of this research.

Chapter 6 provides a brief summary of the new capabilities in carrying out surface analysis experiments on MALDI prepared samples.

Conclusions are drawn in Chapter 7, the final chapter of this thesis.

CHAPTER TWO

INSTRUMENTATION

Prior to the start of this project, a time of flight secondary ion mass spectrometer was in place for academic and industrial use at the Image and Chemical Analysis Laboratories (ICAL) of the Montana State University Physics Department. The main objective successfully completed in this research is the interfacing of a N_2 laser for modifications purposes to develop capabilities in carrying out mass spectroscopy experiments using other methods of surface analytical tools introduced in the previous chapter of this thesis. This chapter will first describe instrumentation that was already in place prior to the start of the project. Then the modifications put in place in order to complete the objectives of this research will be described.

Existing Instrumentation Prior to this Research

The existing spectrometer [model: TRIFT I (TRIple Focusing Time-of-Flight), by PHI-EVANS] is a state-of-the-art mass spectrometer with two primary ion sources, a pulsed Cs^+ source as well as a pulsed focused liquid Ga^+ gun. For SIMS experiments carried out under the scope of this project, the Ga^+ gun was employed exclusively as the primary ion source. This source is capable of providing pulsed energetic (in the range of 5 kV- 25kV) Ga^+ ions. For the majority of experiments in this research, 15 kV Ga^+ ions were used. The ion

beam is focused to submicron size and rastered across a predetermined square area on the sample surface. The dimension of the rastered area is user controlled. Regions ranging in area from [50μm × 50μm] to [200μm × 200μm] were typical throughout this research. As a result of this bombardment by Ga^+ ions, secondary atomic and molecular species are desorbed from the vicinity of the primary ion impact region. Ionized portions of these secondaries, which are representative of the chemical structure of the analyzed area are then electrostatically accelerated by applying approximately 3 kV to the sample substrate and keeping the extraction plate at ground potential.

The ion-optics column of the TRIFT I system guides the extracted ions via an immersion lens. The extracted ions are transported via a transfer lens to a series of three 90° hemispherical electrostatic analyzers (ESA's). The ESA's provide energy focusing by the means of kinetic energy compensation for ion flight times and imaging purposes [12]. A schematic of the TRIFT I system is presented below.

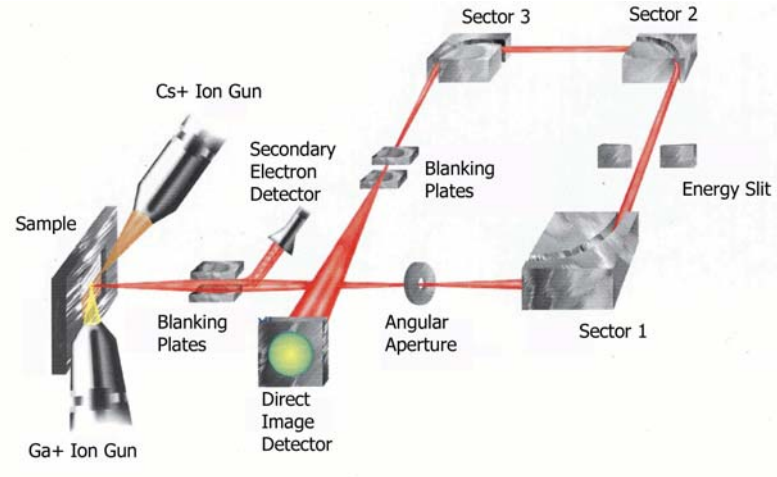

Figure 2.1 A simplified schematic of TRIFT I.

Recalling Eq. (2.12), the expression for the secondary ion arrival times as they strike the detector is given by:

$$TOF \cong t_a + D\sqrt{\frac{m}{2qV_0}} \tag{2.1}$$

where D is the total effective distance traversed by the ions (D ≈ 2m, the length of the spectrometer flight tube). A time-to-digital converter (TDC) with a time resolution of 156 ps is used for time and ion detection [12].

One of the most useful features of the TRIFT I system is the ability to provide imaging of the detected secondary species. This is accomplished by the combination of energy-focusing ESA's and the feature of the system that allows for the registering (x,y) raster position of the primary ion beam on the surface of the sample. The raster position is then correlated to the secondary ions originating from this region and reaching the detector. The TRIFT I system also allows for different schemes of data storage. One such scheme is retrospective analysis, where the user is able to collect a mass spectrum, store this spectrum along with the (x,y, t) positions of every detected secondary ion and give the user the ability to replay these stored data. Each pixel of the 256x256 pixel area contains a full mass spectrum from that point and each mass region of this spectrum as a function of time is accessible by the user once the raw data is collected. As such, in retrospective analysis, one is able to recreate a mass spectrum from any user-defined region on the ion image. TRIFT I uses WinCadence software, distributed by PHI, to operate all aspects of the

instrumentation other than sample introduction. In what follows, a description of the modifications done on the existing system, and the capabilities of the new combined system is offered.

LASIMS (Laser-Assisted Secondary Ion Mass Spectroscopy)

To make the TRIFT I instrument compatible with the principles of LDMS and MALDI experiments as outlined in the first chapter of this thesis, a laser source had to be interfaced to the existing instrumentation. Since the laser source was installed simply as an additional analytical probe, in addition to the existing Ga^+ and Cs^+ ion primary ion sources, the original design of the spectrometer hardware did not need to be altered. Other considerations associated with the laser primary source, however, had to be addressed. These included timing issues regarding the temporal synchronization of the new source with the existing hardware. Since the mechanisms of desorption and the subsequent ionization of secondary species resulting from photon bombardment are different in nature than that of energetic primary ions, data acquisition, and subsequently the analysis of the data collected, were among issues having to be addressed.

LASIMS EXPERIMENTAL SETUP

A diagram illustrating the experimental setup is presented below in Figure 2.2. For the laser source, a N_2 laser (VSL-337-ND, by Laser Science International, Newton, MA) lasing at λ = 337.1 nm was employed. This source

was placed on an optical bench next to the TRIFT I spectrometer assembly. After the beam passed through a variable aperture (iris), it was incident on a lens with a focal length of *f* = 1 m. Next on the optical path was a filter wheel, complete with 5 optical filters of different attenuation values. The transmission values of these filters at 337.1 nm are given in the table below. An appropriate filter value was chosen depending on the nature of the sample being analyzed.

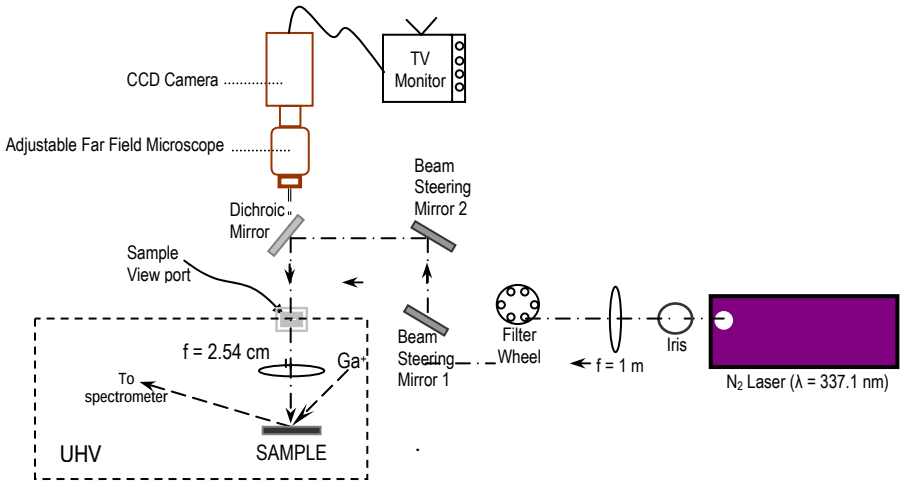

Figure 2.2 LASIMS experimental setup

Filter No.	% Transmission @ 337.1 nm
1	100 (No Filter)
2	1.1
3	12
4	22
5	48
6	72

Table 2.1 Transmission for the 337.1 nm wavelength for the filters included in the filter wheel assembly of the LASIMS setup.

After being steered by two mirrors, the laser beam is guided to a dichroic mirror and ultimately into the sample chamber of TRIFT I through a glass viewing port. The beam is focused by an *f* = 2.54 cm lens onto the sample surface inside the chamber. While reflecting 337.1 nm into the spectrometer sample chamber,

the dichroic mirror transmits visible wavelengths away from the spectrometer, allowing the inspection of the sample via a video zoom camera on a TV monitor.

After the laser beam is directed onto the surface of a sample in the sample chamber of the TRIFT I, certain alignment-related issues have to be addressed. Most importantly, if the existing hardware is going to be used, one must make sure that there is perfect spatial alignment between the Ga^+ particle beam and the laser beam. Furthermore, before any analysis is possible, the user has to be certain about the location of the incident beams on the sample surface, which is being bombarded with the multiple beams. This alignment is made possible by the observation of physical changes brought upon surfaces due to sputtering by either beam.

In this system, alignment is a three-step process. First, the Ga^+ beam impact area on the sample surface must be identified on the TV monitor. Next, a relatively high intensity laser beam is allowed to strike the sample surface, leaving behind a visible spot observable by the video camera. Finally, complete superposition of the two beams is implemented by moving the alignment mirrors and visually verification on the monitor. The following will describe the beam alignment process for LASIMS.

Particle beam alignment

With the particle beam, operating the Ga+ gun in a continuous (DC) mode can bring upon changes to the physical appearance of the surface of the sample and often times steps can be taken to visually verify this on the TV monitor. As

explained later in this thesis, this technique is usually employed for ‘depth profiling’ experiments. In the ‘depth profiling’ mode of operation material is actively removed from the analysis area, and this is damaging to a surface. Therefore, when using this method, only a small area on the sample surface that is not critical for analysis purposes should be chosen as to not ‘waste’ any meaningful region and data. Furthermore, this DC ion beam should bombard the surface for the shortest amount of time possible. For example, a rather small raster size (50 x 50 μm2) can be etched with continuous Ga+ for a duration of 5 seconds resulting in an imprint of this etched area, which is readily visible on the TV monitor, identifying the impact area of the Ga+ beam on the surface. This method is very practical, especially with smooth surfaces such as Si wafers. For instances where the imprint image is not easily obtained on the TV monitor, the surface can be plasma-deposited with a thin layer of gold, which aids in creating a visual contrast between the etched and undisturbed areas on the sample surface. For rough surfaces, such as geological samples (clays, soil, etc.), it may not be possible to obtain such an image in a practically short amount of time. In these cases, interesting features on the sample surface may be used to locate the Ga+ beam. Such features of interest include islands, corners and channels on the surface, which are visible on the TV monitor. Acquiring an ion image of these samples with the TRIFT I system and correlating the features with the image visible on the TV monitor will enable the user to know the exact region on the surface that is being bombarded with the particle beam.

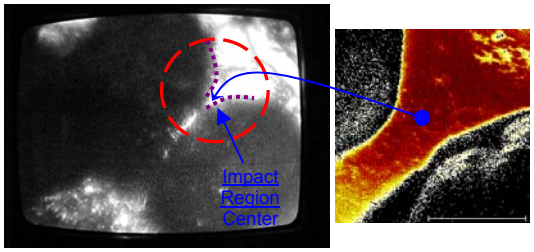

Figure 2.3 Locating the particle beam impact region on the TV monitor for a rough mineral sample surface. The sample is a clay mineral on an Indium substrate. The secondary ion image corresponds to the indium signal. In the TV monitor, the light areas correspond to the substrate, and the dark regions are the clay minerals.

Laser Beam Alignment

The first order of business in the alignment of the laser beam involves merely bringing the beam onto the sample surface. The most crucial step of laser beam alignment is the minimization of the angle θ_r. This angle, as illustrated in the Figure 2.4 below corresponds to the angle with which the beam is reflected from the view port through which the laser beam enters the experimental chamber via a reflection by the dichroic mirror. The beam should enter the chamber as close to perpendicular as possible.

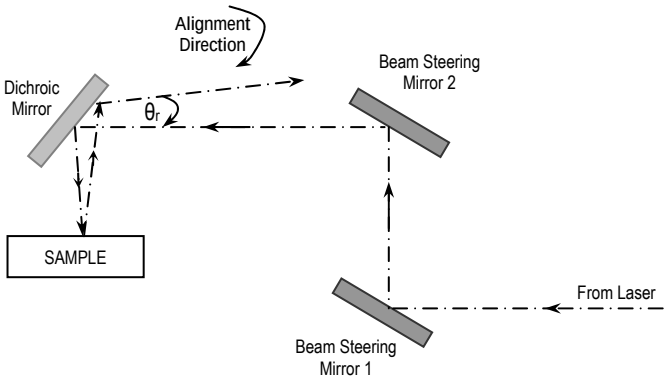

Figure 2.4 The rough alignment for the laser beam. This procedure ensures that the laser beam is incident on the sample. The only remaining task after this procedure to complete alignment is to steer the laser beam to the same location being bombarded with the particle beam.

The first step in the alignment process is to make sure the laser is incident on the dichroic mirror and ultimately into the sample chamber. Since the wavelength of the laser is invisible to the human eye, a white piece of paper can be used to cover the mirror and visually inspect that the beam is in fact incident on the mirror. Subsequently, one must find the beam reflected from the glass viewport. Again using a white sheet of paper, this time in front of Beam Steering Mirror 2, two laser spots can be identified. The weaker of the two spots corresponds to the reflected beam. To minimize the reflection angle, beam steering mirrors may be horizontally and vertically adjusted until the reflected beam is very near to the incident beam.

Unlike in the case of the particle beam, it is less challenging to spot the laser beam impact region on the TV monitor. At points of impact, especially at high intensities, the laser beam ablates material from the surface. The ablated area is easy to identify on the monitor. In cases where the laser-ablated area is not easy to spot, one can adjust the intensity of the beam by choosing a filter that transmits more of the beam.

<u>The superposition of the laser and the particle beams</u>

Once the impact regions of the laser and the particle beam are identified on the TV monitor, the final phase of beam alignment can be implemented. In this final phase, the Ga^+ alignment is undisturbed because it was prealigned with the physical location of the extraction aperture. Hence it is necessary to move the

laser beam is to overlap with the particle beam. This is achieved by making small but precise adjustments with the beam steering mirrors.

After the alignment process is completed, the particle and the laser beams will coincide spatially on the sample and as a result, either beam will probe the same surface location. Photographs of the TV monitor at different alignment steps are given in the figure below.

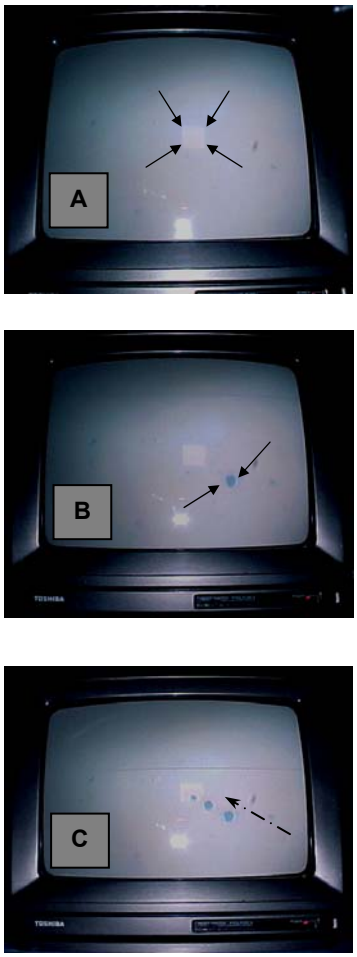

Figure 2.5 Procedure for the particle and laser beam superposition. First, the impact region of the particle beam on the sample surface is identified (A). Next, the laser beam is brought onto the sample surface (B). Finally, using beam steering mirrors of the LASIMS setup, the laser is moved over to the Ga^+ beam impact region (C).

Instrument Control

The LASIMS setup required the use of additional instrumentation to address critical issues relating to timing as well as data acquisition and analysis. While some of this instrumentation included familiar laboratory equipment such as a digitizing oscilloscope and a digital delay/pulse generator, others had to be custom-built specific to this project. For such instruments, the virtual instrumentation environment of LabVIEW was employed. LabVIEW was also used to link and control all new instrumentation installed as a part of this project. The programs developed for this project are included in a CD, are submitted as a part of this thesis.

A Brief Introduction to LabVIEW

LabVIEW is a graphical programming environment developed by National Instruments. This platform utilizes G, a graphical programming language. G differs from conventional languages, which use lines of code to implement functions, in that the 'G' programmer wires icons to create an application.

There are two accessible portions that make up a LabVIEW program: The front panel and its associated block diagram. The front panel is the only accessible portion of a program during its execution. Its appearance emulates a real physical instrument complete with displays, knobs, gauges and buttons. For this reason, LabVIEW programs are referred to as virtual instruments (VIs). Building a front panel that resembles a real hardware instrument performing

similar tasks is the first step in creating a standard LabVIEW VI. Subsequently, the user creates the source code that implements the functions required of the VI by building a block diagram. A very simple front panel and its associated block diagram are presented below in Figure 2.6.

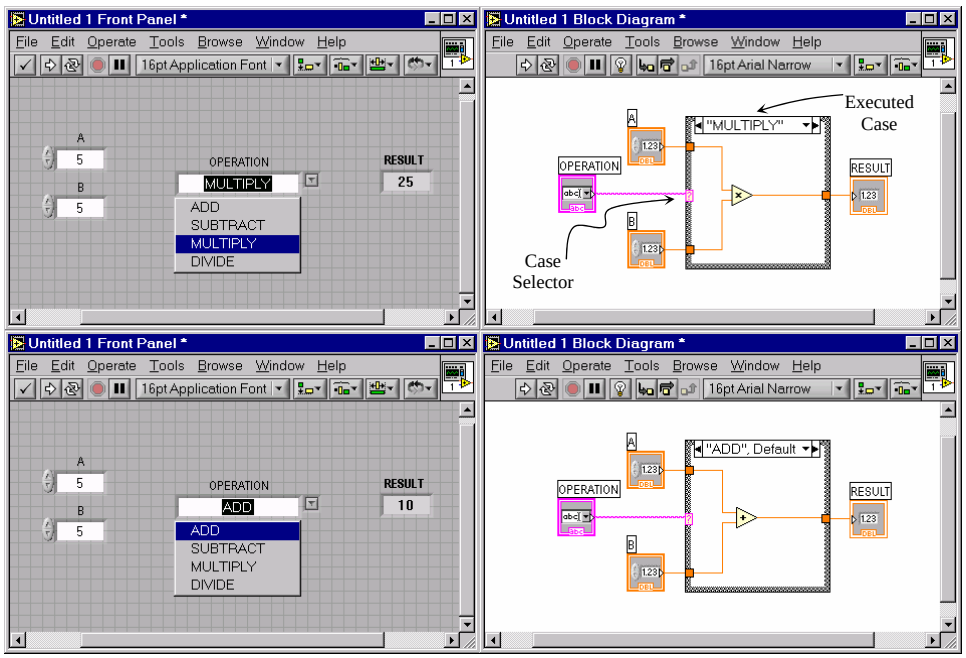

Figure 2.6 A basic LabVIEW code to perform simple arithmetic operations on two numbers.

In the above example, there are 3 control (A, B, Operation) terminals and 1 indicator terminal in the front panel. Two numbers, as entered by the user in the A and B control terminals undergo the arithmetical operation as specified by the user. The result is displayed in the indicator terminal, 'RESULT', in the front panel. Making up the associated block diagram is the necessary source code needed to implement these arithmetic operations. The actual operations are part of a case structure, the G equivalent of an if-then statement. The case selector (if) is set by the user input of 'OPERATION' in the front panel.

The versatility in programming along with its specialized libraries developed for the purposes of instrument control made LabVIEW a sound choice as the platform on which to develop customized instrumentation. LabVIEW communicates with and controls external instruments with GPIB (General Purpose Interface Bus) standards. The parallel nature of the GPIB bus allows communication with multiple instruments at the same time.

New Hardware

TDS3054 Four Channel Color Digital Phosphor Oscilloscope

One of the most crucial instruments used in this project was the Tektronix TDS3054, a 500 MHz, 5 GSamples/s, four-channel oscilloscope. The use for this instrument is two-fold in this project. First, the scope was used as a mass spectrum-recording device. This mode of operation for the scope will be explained further in the data acquisition section of this chapter. Second, the TDS3054 was used for displaying the waveforms associated with the temporal alignment of analytical probes. In the LabVIEW environment, any signal on the oscilloscope display can be downloaded to the computer via the GPIB interface. The downloaded signal will be represented as a two-column array, with a 10,000 data point resolution.

DG535: Four Channel Digital Delay/Pulse Generator

One problem that arises when one wishes to introduce a laser source, as an additional analytical probe to an existing SIMS unit is trigger synchronization.

Nominally, the Ga^+ source of the SIMS instrument is triggered at 8 kHz. This frequency range corresponds to a mass range of 0-2090 amu. Since it was the goal of this project to take advantage of existing hardware associated with the spectrometer, it was crucial for the laser source to be compatible with the timing sequences of the existing unit. This is accomplished by the perfect synchronization of the laser-triggering scheme with that of the Ga^+ source.

The technique used here to achieve the synchronization utilized a digital delay/pulse generator (Model DG535-SRS, Inc.) In this scheme, the pulse generator was used for the perfect overlap of pulses used for Ga^+ triggering and the laser triggering.

The DG535 is capable of producing four precise logic-timing transitions. These channels can also be configured for the generation of two precisely controlled pulses. This generator can be internally or externally triggered. The unit possesses five delay output BNC's, labeled A, B, C, D and T_0. T_0 marks the start of any timing cycles for the unit. In cases where the unit is triggered externally, there is an 85 ns delay between the external trigger and the T_0 output. Each of the other delay outputs can be set with respect to T_0 or with respect to each other in 5 ps intervals up to 1000 seconds. In addition, four pulse outputs are also included with the unit: AB, -AB, CD, and -CD. The operational procedure of the unit allows the user to define pulses with two delay channels providing the start and stop times of the pulse. Furthermore, the unit allows for the 'linking' of channels to each other. This feature allows for modification of the channel A without disturbing the width of the pulse available at the AB, or –AB

BNC connectors. The following timing diagram of Figure 2.7 demonstrates the DG535 timing scheme

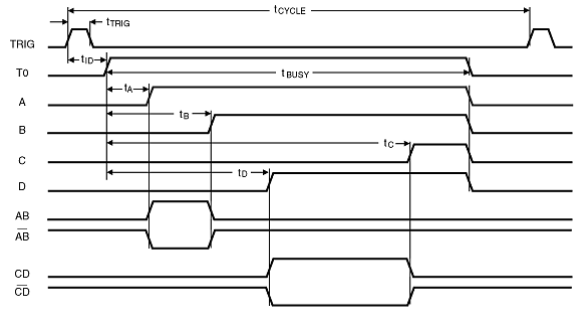

Figure 2.7 The timing diagram for the DG535.

As an example, the setting:

$$A = T_0 + 0$$
$$B = A + 450 \text{ ns}$$
$$C = B + 2\ \mu s$$
$$D = C + 3\ \mu s$$

will result in the following two waveforms:

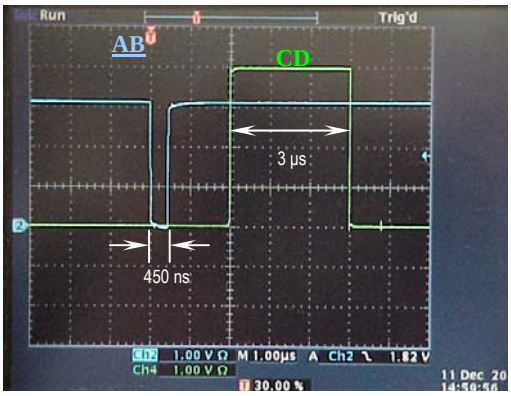

Figure 2.8 The waveforms associated with the timing example given above.

The LCD display of the DG535 is partitioned into 20 (0-19) slots. In the time delay adjustment mode, slots 4 thru 19 represent digits that are used to modify the time delay. To adjust the time delay, the cursor is moved to the

appropriate time slot, and this digit is incremented or decremented to the desired value.

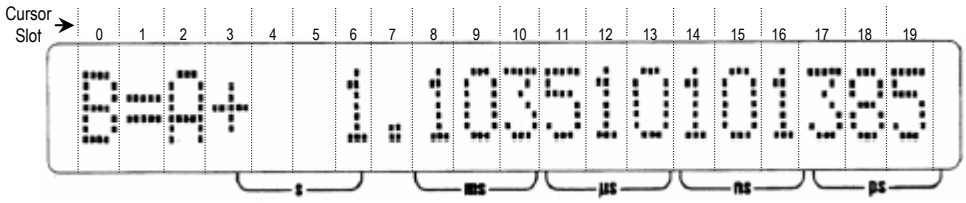

Figure 2.9 The DG535 display.

The first challenge in the synchronization process arises from the rate mismatch between the triggers of the Ga^+ source and the laser. The maximum repetition rate that one can operate this particular laser is 20 Hz, whereas the nominal repetition rate of the Ga^+ source is 8 kHz. The DG535 can solve this problem however, by triggering the unit at submultiples of the triggering source. The unit accomplishes this by the fact that once the DG535 is triggered, it will ignore all other triggers until the longest delay channel of the unit has timed out. Therefore, the unit can be externally triggered with the original Ga^+ source trigger, the longest delay of the unit can then be set to about 50 ms, which corresponds to 20 Hz, and can effectively be used as a frequency divider, providing an output at one of its pulse BNC outputs. This output can then serve as the reference trigger for the modified system.

The next task after obtaining a new reference signal is the generation of the actual signal to be used as the trigger for the laser. The constraint associated with generating this signal is the requirement that the laser beam must arrive at the sample surface at the same time with the Ga^+ ions. The

different paths traversed by either primary beam along with differences in their velocities require that to achieve such temporal synchronization, steps need to be taken in defining the correct timing scheme of the laser trigger. In the experimental setup of the LASIMS system, this meant that the laser trigger lagged the reference beam to ensure that both beams arrived at the sample at the same time. After numerous experiments, it was determined that the difference in time between the Ga+ ions and the laser light to reach the sample was 1.363 μs, with the laser light arriving first. The laser trigger pulse, as generated by the DG535 was linked to the reference signal. This synchronization meant any modification done on the reference signal delay settings did not affect the laser trigger pulse width; the two signals moved in time synchronized to each other.

Perfect overlap of the original Ga^+ gun trigger and the newly generated reference pulses eliminates any concerns about the calibration of spectra produced by laser irradiation. To maintain this perfect overlap however proves to be a challenging task. There are issues of accuracy, timebase drift, and jitter associated with the DG535 instrument. These concerns prevent the user from keeping the perfect overlap once it is achieved. Furthermore, to be assured of the validity of any spectrum, immediately before obtaining any spectra, the user must make certain that perfect synchronization exists as an initial calibration. To address these issues an effective and practical solution was needed. The solution was created using the LabVIEW platform.

LabVIEW Code for the Temporal Alignment of Analytical Sources

The Alignment VI is implemented by first creating a replica of the pulse train that is used to trigger the particle beam of the TRIFT I. In the TRIFT system, this pulse, labeled *Prate0* functions as the reference signal for all other timing events. As mentioned above, the first challenge in alignment arises from the fact that there is a frequency mismatch between the nominal repetition rate of the particle beam and that of the laser. To create a frequency divided replica of Prate0, the DG535 is externally triggered with *Prate0*. Subsequently, the delay of one of the channels, in this case Channel *C*, is set to 49 ms, which will force the unit to disregard all other triggers until the delay of Channel *C* has timed out. Next, by noting that the pulse width of *Prate0*, Channel *D* delay is set to 432 ns. Now the *CD* output of the DG535 will provide a frequency divided version of the original *Prate0*, *Prate0'*, with a frequency of 20 Hz and a 432 ns pulse width identical to he original particle beam trigger. *Prate0'* can now be used to trigger the Ga^+ gun at a slower rate. The next task in the temporal alignment process involves the overlapping of the original and the frequency divided reference pulses. Although the replicate pulse is generated directly from the original pulse, certain limitations associated with the DG535 prevent maintaining the perfect overlapping of the two pulses once it is achieved. These limitations are in large part due to the timebase drift of the instrument. This drift is a function of the instrument temperature and the limitations it poses are more pronounced if the instrument is not warmed up. In addition, over several hours of operation, which was typical in experiments carried out as a part of this project, timebase drift is

an important issue having to be addressed. A LabVIEW code was written to address this problem.

The alignment code written in LabVIEW first sets the time delay of channel *C*, corresponding to *Prate0'* as mentioned above, to a nominal value. For 20 Hz (max. rep. rate for the laser), the channel *C* delay is set for 49 ms. If the laser was needed to operate at 10 Hz, then channel C delay would be set for 99 ms and for a 5 Hz repetition rate 199 ms is appropriate. Next, the two waveforms are displayed on TDS3054 screen.

The two waveforms representing the *Prate0* and *Prate0'* are both negative pulses of identical width. To align these two pulses, one possible approach is to identify a reference point common to both pulses, and to make certain that these reference points appear on the same time slot on the oscilloscope display. Since the two waveforms are negative pulses, one such reference point choice is the minimum value of the derivatives of either pulse. The minimum value for the derivative of a negative pulse appears about the midpoint of its leading edge. In this project, the two pulses on the oscilloscope display were downloaded and brought into a PC environment as two two-column arrays. After the download process, a derivative-calculating LabVIEW utility was employed. The calculated derivative values were again stored in two arrays. Next, the minimum values of the two arrays were located in terms of their sample numbers. After these sample locations were converted into time units, the absolute difference in time between the two reference points were calculated. The code written to alleviate the time mismatch was a multiple iteration process. As an example, for a 123 μs

hypothetical time difference between the reference points, the DG535 cursor would be remotely moved to slot 11 of channel *C* delay menu via the GPIB interface, and this digit would be incremented or decremented depending on which waveform was leading the other. This way the hypothetical time mismatch would be reduced to 23 μs. Next, the cursor would be moved to slot 12 and this digit would be adjusted twice to reduce the mismatch to 3 μs. The process would be repeated until an acceptable time difference was obtained.

This alignment code was run prior to the collection of any spectrum during the project. The code achieves alignment usually in less than one minute and it also serves as an initial mass calibration. The user is able to visually verify the two waveforms locking into alignment on the oscilloscope and the computer screen. A message is displayed on the oscilloscope display when the two waveforms are in sync.

Data Acquisition, Analysis and Display

Although most of the data acquisition, analysis and display associated with this research could be performed by the WinCadence software of the original instrument, introducing the laser source as an analytical source brought upon a need to modify these capabilities. The original software displays mass spectrum secondary ion intensity in arbitrary units and the analysis of secondary counts could only be done qualitatively.

In an effort to improve analysis capabilities, a LabVIEW program was created. The main advantage introduced by this new program is the ability of

downloading mass spectra directly from the oscilloscope, where the intensities associated with detected secondary ions were displayed proportional to the charge received by the channelplate detector, rather than event counting as it is the case in the pulse counting scheme of the original TRIFT WinCADANCE software. The pulse heights are completely ignored in the WinCadence. For example, if more than one identical mass arrives at the detector at the same time, WinCadence will register only a single pulse, while the oscilloscope will receive proportionally larger pulse, taking into account the multiple charges arriving at the detector for a given nominal mass. The possibility of generating multiple particles at the same mass as a result of a particle primary pulse is not an issue in ToF-SIMS but the high fluence laser beam can easily generate multiple particles at a given mass as result of laser excitation.

Yet another advantage of this code is the fact that it was custom designed for a laser source acting as the primary analytical probe. In that sense, the user is able to set the appropriate number of laser pulses to collect a mass spectrum. This is an advantage, in that the user is able to control the start and the stop times for collecting spectra with the laser source. Generally, a standard dose of 300 laser shots was chosen to record a complete spectrum.

In the standard setup, mass spectra were collected by triggering the oscilloscope with the 20 Hz replicate reference signal, Prate0'. The triggering channel was Channel 2 of the four channel oscilloscope. Mass spectra signal was recorded by connecting the microchannel plate detector output of the spectrometer to Channel 1 of the oscilloscope. ToF spectra could be viewed

both on the oscilloscope display and the computer screen. The user has the ability to define the mass range over which spectra is to be collected by adjusting the ‘record length’ control on the front panel. Additionally, the user has the ability to control the scaling of the vertical axis. Often times this is essential in displaying a meaningful spectrum.

Another important function performed by this program is time-mass conversion associated with spectra. This is accomplished in two phases by the program. First, the mass spectrum displayed on the oscilloscope screen is downloaded to the computer via the GPIB interface and the LabVIEW code. This mass spectrum is brought into the LabVIEW environment as a two-column array in terms of voltages and sample numbers defining each data point making up the spectrum. LabVIEW code converts the sample numbers into time stamps by noting the horizontal display parameters of the oscilloscope. This information is stored in another two-column array. Second, the program converts the time stamp values to mass units with an equation calculated by using the relationship of Equation 1.13d.

$$\sqrt{m} = a \cdot TOF + b \tag{2.2}$$

The time-mass conversion equation used by LabVIEW was calculated by using the parameters associated with two peaks of known flight times. The two peaks used were Na (m = 22.989767 amu) with a flight time of 14.41 μs and Au (m = 196.966543 amu) with 38.53 μs time of flight. Solving the system:

$$\sqrt{22.989767} = (14.41\times10^{-6})a + b$$
$$\sqrt{196.966543} = (38.53\times10^{-6})a + b$$

yields

$$a = 383073 \quad amu^{\frac{1}{2}}s^{-1}$$
$$b = -0.725312 \quad amu^{\frac{1}{2}}$$

The time-mass conversion equation is therefore:

$$\sqrt{m} = (383073\cdot TOF) - 0.725312$$
$$or$$
$$m = (1.46745\times10^{11})\cdot(TOF - (1.89341\times10^{-6}))^2$$

Perhaps the most crucial analysis in inspecting a mass spectrum is the analysis of individual peak parameters making up the spectrum. This capability was included in this program by introducing horizontal and vertical bars on the mass spectrum display. There are multiple operations performed by these bars. First, the integral of a peak can be calculated by positioning the bars so that the peak of interest is between the cursors. The integration method (Trapezoidal rule, Simpson's rule, Bode rule) used is user controlled. The user has the ability to set two integrals, one for spectrum and one for noise associated with the spectrum. The program calculates the net integral associated with a peak by subtracting the noise from the meaningful spectra. Secondly, differences in amplitude and mass between two peaks can be calculated and displayed on the computer screen. An example of this VI front panel is presented below.

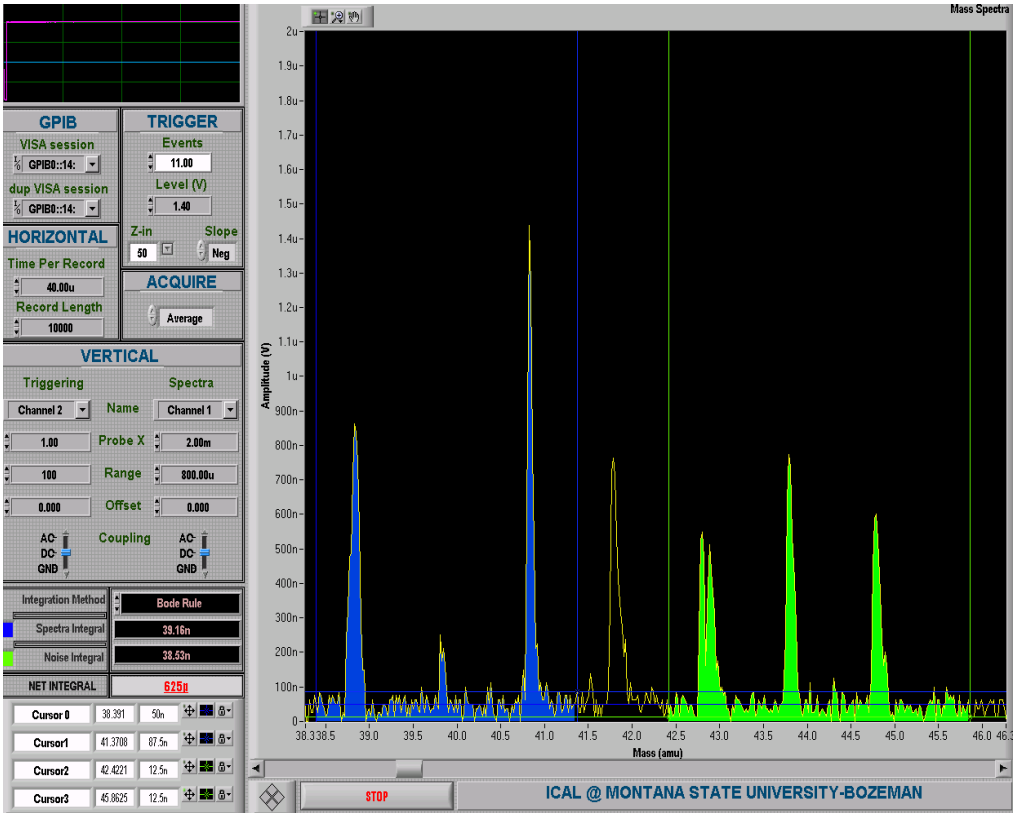

Figure 2.10 The front panel associated with the data analysis VI of the LASIMS setup.

CHAPTER THREE

LASER CLEANING

A considerable number of materials analyzed with SIMS methods are electrically insulating. Since the early days of SIMS, analyzing such samples has posed great practical difficulty. This is due to sample charging which makes it difficult to establish a stable surface potential during analysis [14]. One of the advantages of the modified system is the ability it offers its user in conducting rapid and practical surface analysis on this family of materials thanks to the availability of dual pulsed complementary primary particle beams and a laser source.

When focused primary gun ions, such as Ga^+, bombard the surface of an insulating material, secondary ions and secondary electrons are emitted from that insulating surface. Given the poor conductivity that is the characteristic of insulating materials, any charge that is deposited in the sample cannot be transported from the surface. The net result is the accumulation of typically positive charge of the sample in question. A typical sample holder arrangement used for SIMS analysis of insulators is presented below in Figure 3.1.

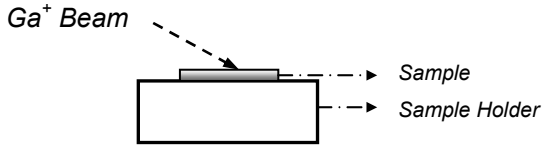

Figure 3.1 A typical sample holder arrangement used in the SIMS analysis of an insulator. The sample is housed in ultra high vacuum (UHV) environment.

To obtain meaningful a mass spectrum from an insulating sample, a scheme to alleviate the built-up charge on the sample surface is necessary. In what follows, an equivalent electric circuit is introduced to describe the charging problem. Additionally, ways of compensating for this charge build-up encountered during the analysis of insulating materials are discussed.

The effects of ion bombardment of an insulating surface, the resulting charge build-up and the necessary discharge of the build-up can be simulated with a three element equivalent circuit consisting of an ideal current source and a parallel RC network [14]. The equivalent circuit is illustrated in Figure 3.2 below.

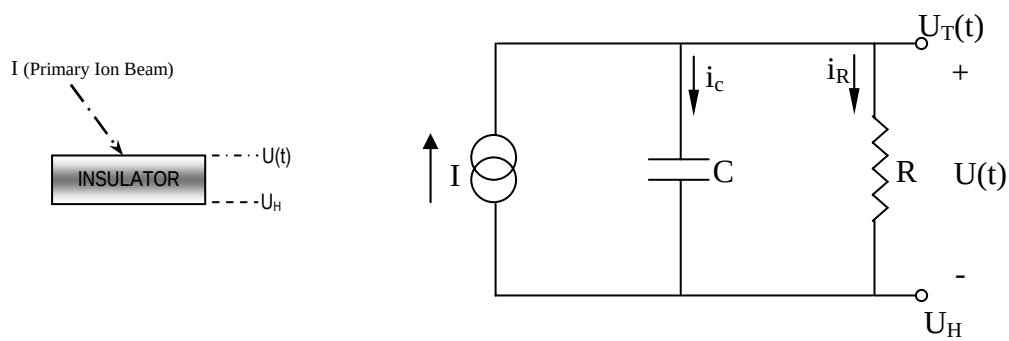

Figure 3.2 An equivalent circuit that can be used to calculate the charging of an insulator under ion bombardment [1].

In the above circuit, the current source represents the primary beam, the capacitor is used to model the charge-up effect and the resistor is included for the discharging of the capacitor.

For a typical sample holder arrangement, U(t) is the potential difference between the opposite faces of the sample. For the ease of analysis, the current source and the parallel resistor can be replaced, via a source transformation, by an ideal voltage source with the same resistor in series.

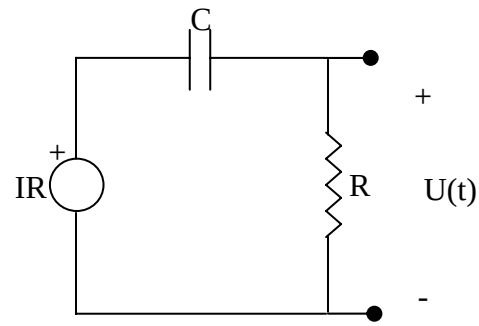

Figure 3.3 The equivalent source-transformed circuit of Figure 4.2.

Subsequently, by Kirchoff's Voltage Law:

$$IR = U + (RC)d\frac{U}{dt} \tag{3.1}$$

The potential accumulated by the surface as a function of time is then given by,

$$U(t) = IR[1 - e^{(\frac{-t}{RC})}] \tag{3.1}$$

Polymers are some of the many insulators often analyzed with SIMS methods. Typical electrical parameters for a polymer are [3]: R ≈ $10^{14}\Omega$ and C ≈ 10^{-14}F. For a routine analysis in the TRIFT I system, an average primary ion current of 42pA bombards an area of 100μm^2 on the sample. Substituting these values into (3) yields:

$$U(t) = 4200 \cdot [1 - e^{-t}] \tag{3.2}$$

Equation 3.2 predicts that charging effects will bring the surface potential of this typical polymer to about 4kV after only 3 seconds of bombardment making it impossible to obtain a stable and meaningful mass spectrum.

Compensation for positive charge build-up on insulator samples and collection of meaningful mass spectra from such surfaces remain to be some of the most challenging tasks in mass spectroscopy today. The undesirable

consequences of surface charging are well documented. Signal instability, peak broadening, signal reduction, variation in intensity ratios of peaks having different energy distributions and complete loss of signal shortly after start of ion bombardment are all negative implications associated with surface charging [15]. A charge build-up will also result in the migration of ions within the sample substrate to the surface, the charging will divert the primary ion beam from the intended analysis area, and sample charging will change the energy distribution of secondary ions and move the energies out of the energy passband of the mass analyzer. Therefore, when performing SIMS analysis of insulating materials, a method of compensation needs to be implemented to address the charge build-up. Modern instruments employ a variety of methods to address excessive charging of insulating samples. These methods vary with the type of SIMS instrument used. In ToF-SIMS instruments, the most widely used method is referred to as *electron flood gun* method. In this scheme, the ion extraction field is periodically is turned off by bringing the sample voltage down to ground potential. The primary ion source is then blanked. Subsequently, an electron beam of low-energy electrons (<20eV) bombards the analysis area, neutralizing any build-up charge. After the flooding of electrons, the extraction field is established once again by raising the sample voltage, and primary ion gun is once again enabled (unblanked). The process is repeated periodically. This complicated process requires precise timing control between the ion source, electron gun and sample substrate bias (Figure 3.4) and the rise times of these must be sufficiently fast to prevent degradation in mass resolution. In the figure

below, Prate0, eTrig1, SampleBias1, eBlank1, and eCycle1 are names given to timing pulses that are used in the TRIFT I system.

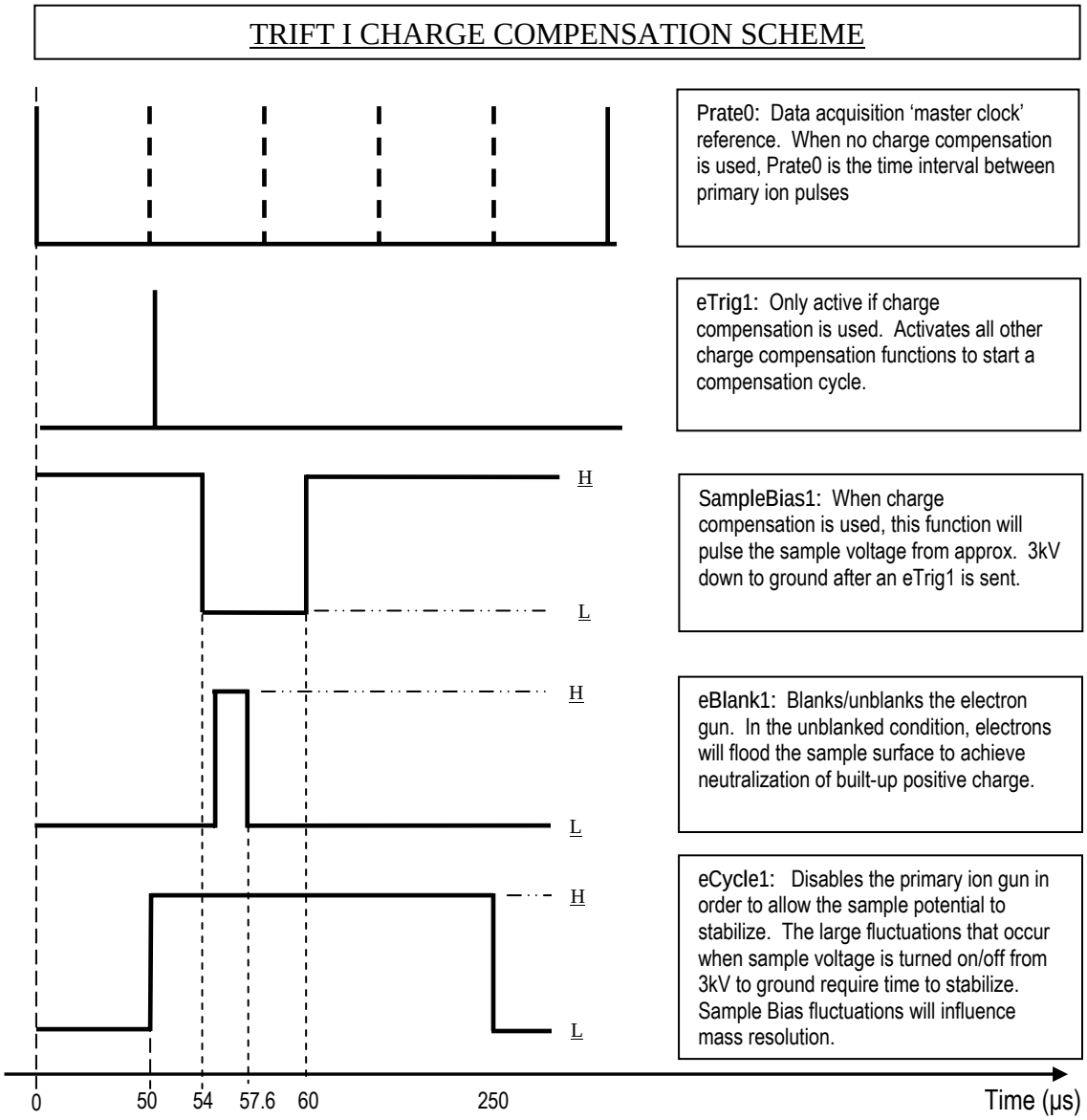

Figure 3.4 A typical charge compensation cycle for TRIFT I. The 'primary' ion gun will pulse, the secondary ions will be extracted and be on their way to the secondary ion detector. Charge compensation cycle will then start with eTrig1. First, the sample voltage will pulse down with the SampleBias trigger. Next, the sample surface will be flooded with electrons. Finally, eCycle1 will disable the primary ion gun for the desired number of pulses. The dashed lines of Prate0 signal signify the disabled primary ion triggers.

Although electron bombardment is a viable method of charge compensation, it is still considerably challenging to perform SIMS analysis of some extremely insulating materials, such as polymers like polyethyleneterephtalate (PET) in a reasonably short time period because of the decreased secondary ion extraction rates due to charging effects.

One way to improve the poor ion extraction is to use a thin metallic grid on the insulating surface to 'pin' the extraction field on the surface. For the TRIFT I system, the grid is constructed from non-magnetic stainless steel with a thickness of 125μm. The use of this method however causes unpredictable ion-extraction performance and in turn poor mass resolution due to the complicated nature of electric fields established by the considerable thickness of the grid near the surface. Near the grid edges the electric fields are perpendicular to the metallic wire surface, giving rise to electric field components parallel to the insulating surface. This causes considerable difficulty extracting the secondary ions from the grid openings. The grid approach is not very practical and it requires considerable amount of time in order to obtain any meaningful spectra. In order to maintain a respectable mass resolution as well as acceptable spatial resolution in the imaging mode, a more suitable method of performing SIMS analysis of extremely insulating samples is needed.

Thin metallic films have long been used to mitigate the charging of insulating surfaces that occurs during scanning electron microscopy (SEM). SEM instruments detect and produce high-resolution images of secondary as well as backscattered electrons emitted from a surface subjected to primary

electron bombardment, which are useful for the characterization of surface topography and for elemental analysis.

A slightly modified version of this same method of thin-film deposition can also be used for SIMS analysis of insulating samples if an effective method of removing a small section of the film is used to allow the chemical characterization of the underlying insulator. The reason that only a small area of thin film is used for removal is because a small area (as compared to separations of the extraction plates) is easier to charge compensate then small openings of a grid over the insulating surface. There are no edge effects nor is there a large area of insulating material to worry about. However, first a small area of the thin film to achieve the desired geometry has to be removed. A limited number of methods exist for such removal. One such method is the sputter cleaning the surface using high-energy ions such as Ar^+ or Ga^+ in order to '*clean*' the thin film. In a ToF-SIMS instrument it is typically the Ga^+ ions that are used to sputter-clean the surfaces. In the sputter mode, a continuous rather than a pulsed beam of Ga^+ ions are used to bombard a samples surface. In contrast to the pulsed mode of operation, a continuous primary beam actively removes material from the top layer of the surface being sputtered. Although very effective in removing a section of thin film, this method also causes severe fragmentation of large molecules that are characteristic of the underlying surface. Thus, the damaging nature of sputter cleaning makes it not an acceptable method of thin-film removal for coated insulators; a more effective method is needed which will selectively remove the metallic film while leaving the underlying insulating material

undamaged. This is achieved by taking advantage of the absorption of light by the metallic film while non-absorbing nature of the insulating material leaving the surface unaffected. As a part of this research, the use of UV laser ablation was demonstrated as a promising tool to clean small areas of gold-coated insulating surfaces such as Polytetrafluoroethyloene (PTFE), and Polyethyleneterephthalate (PET). These areas were then analyzed utilizing the TRIFT I imaging ToF-SIMS instrument and results were compared to the known spectra of these polymers in order to assess the quality of the thin film removal. In Figure 3.5, the severe extent of the morphological damage endured by the polymer sample under analysis as a result of Ga+ sputter cleaning is clearly visible. On the other hand, there is no morphological difference between the laser-cleaned and the undisturbed Teflon surfaces. Laser cleaning is clearly the superior method of cleaning when preserving the morphological features of a polymer surface is of importance. The advantage of laser cleaning extends to the preservation of the chemical signature of the surface as also demonstrated in this chapter.

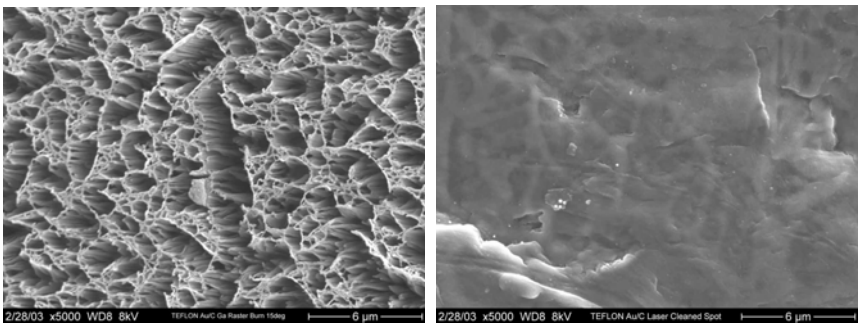

Figure 3.5 An illustration of the two different cleaning methods. The image on the left represents a Teflon sample cleaned via Ga^+ sputtering. The picture on the right illustrates the more efficient and complete cleaning accomplished with the use of an N_2 laser.

In certain cases, imaging SIMS analysis is needed in conjunction with techniques of Secondary Electron Microscopy (SEM) to determine the chemical nature of localized area of interest. High quality images produced by an SEM instrument can be used to identify interesting features on the surface topography of a sample. Subsequently, it is desirable to obtain information of the chemical make-up of these features. To this end, an insulating sample first can be coated with a thin film of a conducting film, usually gold. A high-resolution image of the surface then can be generated to identify interesting features and regions of interest using SEM methods. Next, the sample can be transported to an imaging SIMS instrument, where the previously identified region first can be re-identified. The section of the thin film covering the region of interest on the surface can then be removed by irradiation with a focused laser pulse. We employ a UV laser for cleaning and for spectroscopic purposes (Laser Science, Inc., Franklin, MA, Model: VSL-337ND-S) with a wavelength, λ = 337.1 nm. The focused laser spot on the sample had an approximated diameter of 30μm and provided an irradiance of approximately 1 J/cm^2. With such parameters, one pulse of irradiation was sufficient to remove a section of gold with a thickness of 15 nm. After the thin film removal, a mass spectrum of the region of interest can be collected. Furthermore, a map of the chemical composition of the region can be generated utilizing the imaging capabilities of TRIFT I. The imaging SIMS enables the spatial correlation of the chemical information with the SEM and SIMS images. In this way, the modified system allows for the rapid and complete data collection from a specific location of any insulating surface.

This idea was tested on several polymer surfaces, which can be described as extremely insulating, such as PET, PTFE (Teflon) as well as RTV11 and Intersleek which are polymeric paints used as the top coat of a group of coats to protect surfaces form corrosion and biofouling.

A question of great importance is the extent of chemical damage a sample surface endures as a consequence of laser cleaning. We attempted to first address this problem utilizing the region of interest (ROI) analysis mode of our TOF-SIMS instrument in the analysis of a PTFE sample covered with a 15 nm film of gold. A region on the sample was subsequently laser-ablated with one laser pulse. Spectra were then retrospectively collected only from the laser-cleaned area. These spectra were then compared to widely accepted reference spectra. It was found that collected spectra do indeed agree very well with reference spectra. The laser-ablated region of the surface is shown in Fig. 3.6. Corresponding spectra from the ROI are shown in Fig. 3.7.

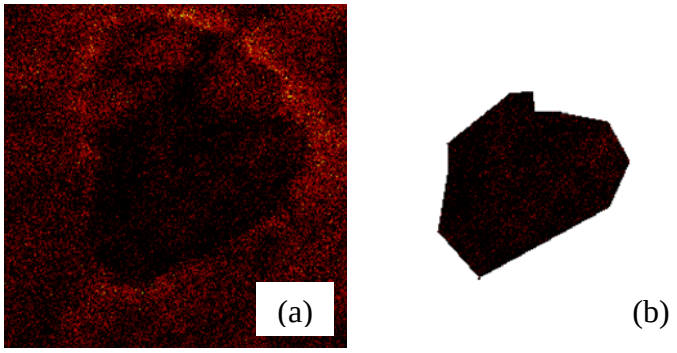

Figure 3.6 Au image of a laser-ablated PTFE sample, (a). The center region on the image, where the Au signal is relatively weak corresponds to the laser-ablated area. The 'Region of Interest', were spectra were collected, (b). Areas on the analysis area that were not laser-ablated are disregarded in the spectrum collection.

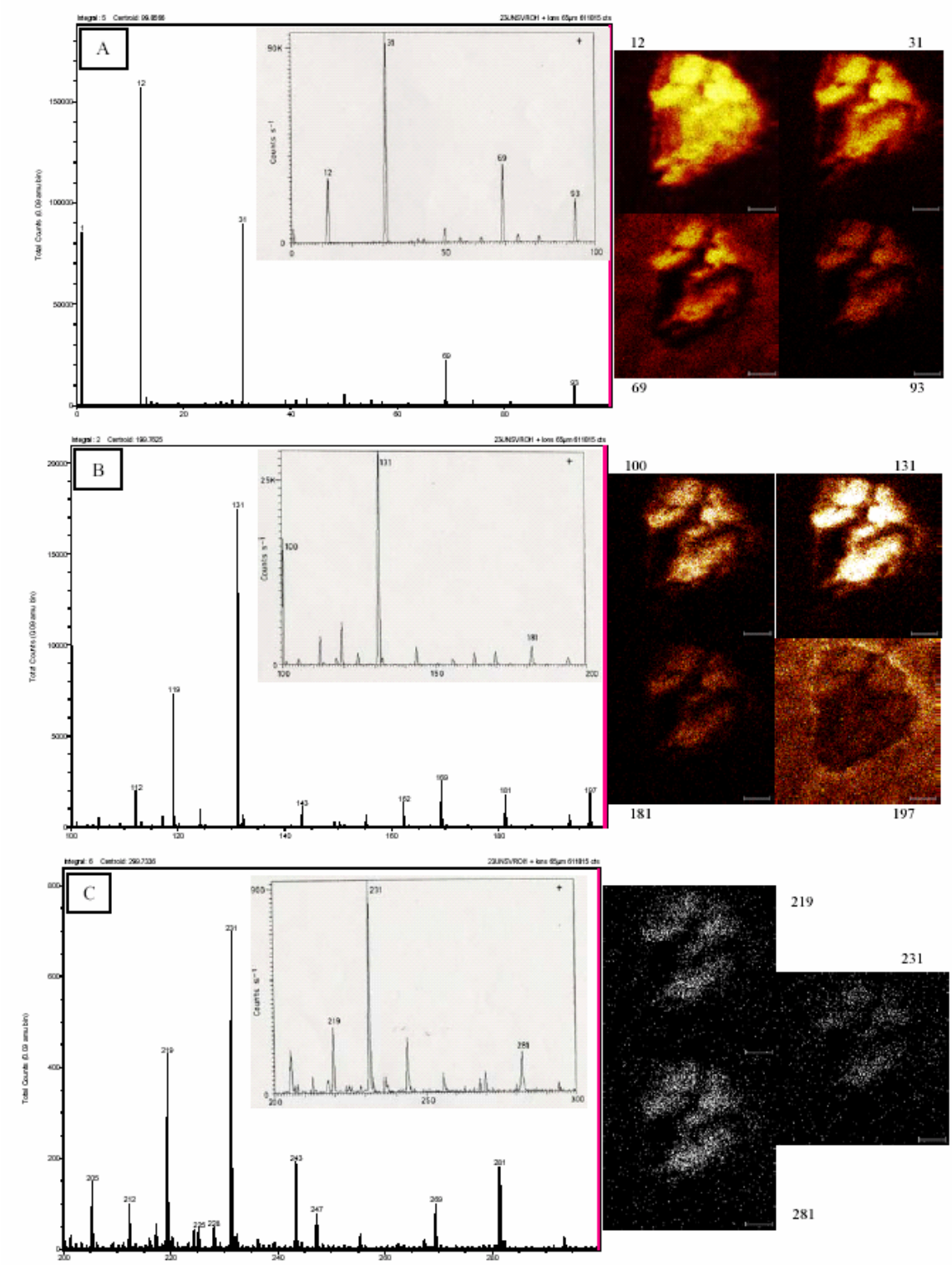

Figure 3.7 The positive ion spectra collected from the 'Region of Interest' and comparisons to the reference spectra. [0-100] amu, (a), [100-200] amu, (b), and [200-300] amu, (c). The reference spectra are presented in the inset.

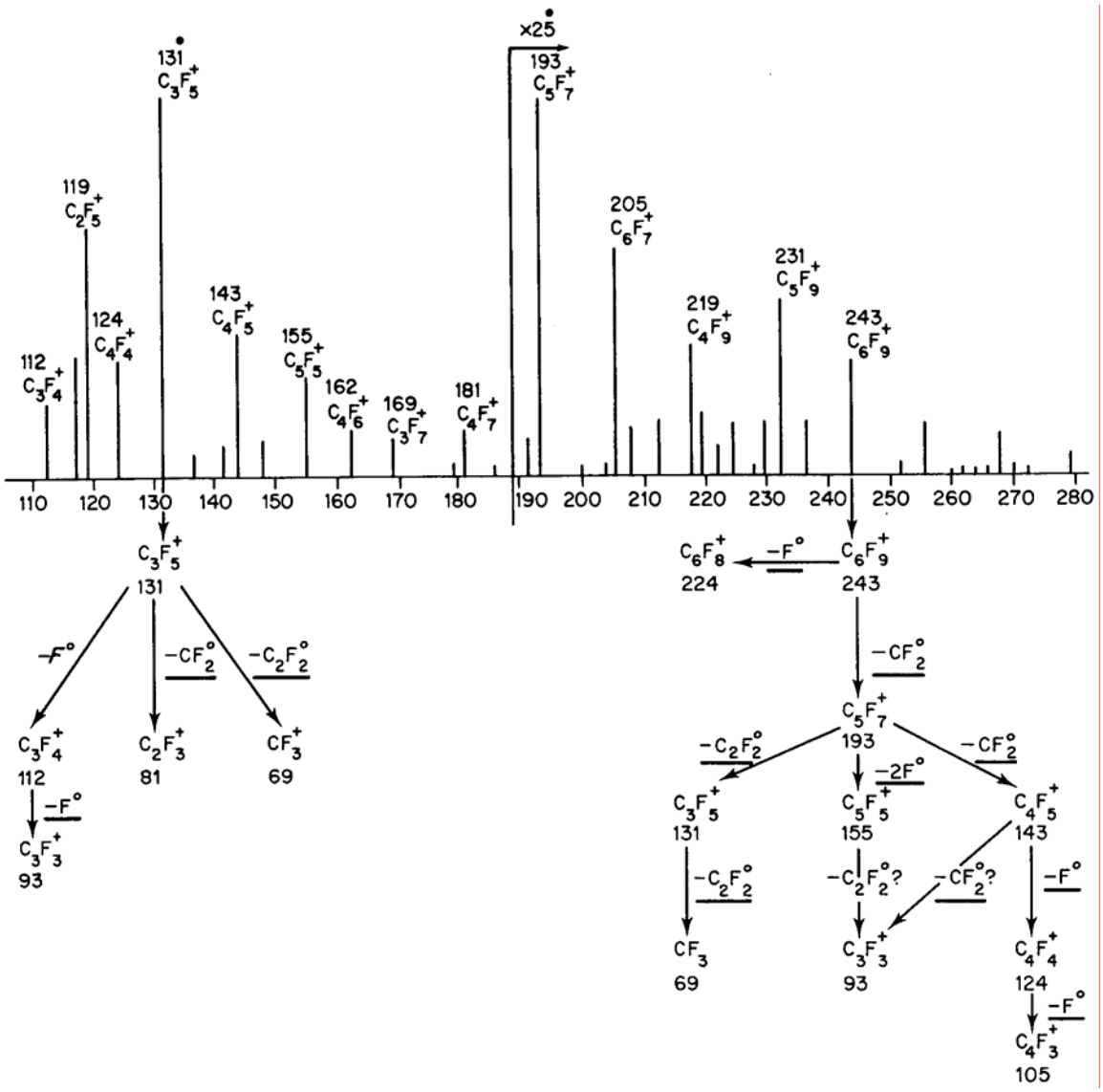

Figure 3.8 Main positive ion clusters of the PTFE polymer. Laser-ablated regions of the PTFE sample analyzed as a part of this research also yielded these clusters emphasizing the undamaging nature of laser cleaning of polymer surfaces [5].

As illustrated in Figures 3.7 and 3.8, the polymer fragments generated from the ablated region are nearly identical for the reference spectra reproduced in the inset.

Comparing mass spectra collected from regions that were cleaned with either method best makes an assessment of the effectiveness of laser cleaning

as opposed to cleaning via Ga+ sputtering. The figure below shows that an area cleaned by laser ablation on PTFE surface yields chemical information with good mass resolution that describes the polymer surface. Laser ablation is clearly the preferred method for preserving the chemical characteristics of the underlying polymer surface.

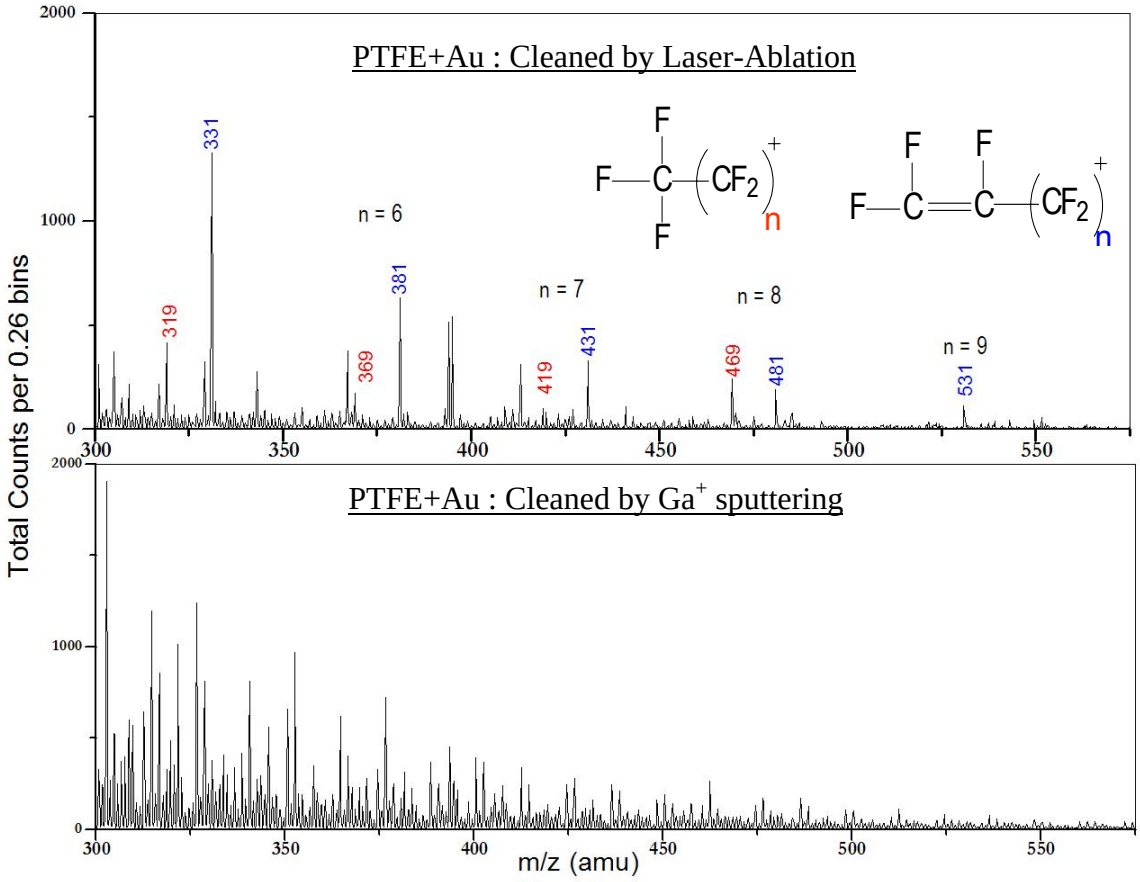

Figure 3.9 Laser-ablation as opposed to Ga^+ sputtering proves to be an undamaging to the chemical signature of the underlying polymer.

Similar ROI analyses were carried out with the common PET polymer. Like in the case of PTFE, an area on the gold-coated sample surface was

cleaned via laser irradiation. Subsequently, negative and positive SIMS spectra taken from the laser-cleaned area were compared to published reference spectra. As in the case of PTFE, it was found that the chemical characteristics of the underlying area were preserved even after laser-ablation. The results are presented below.

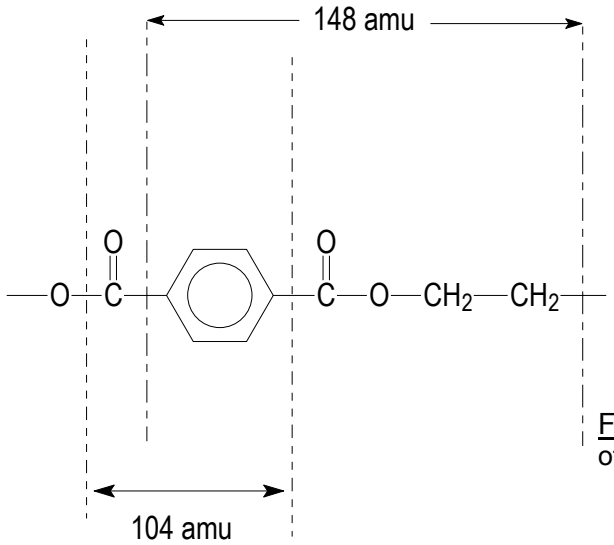

Figure 3.10 Positive ion fragmentation of the PET polymer.

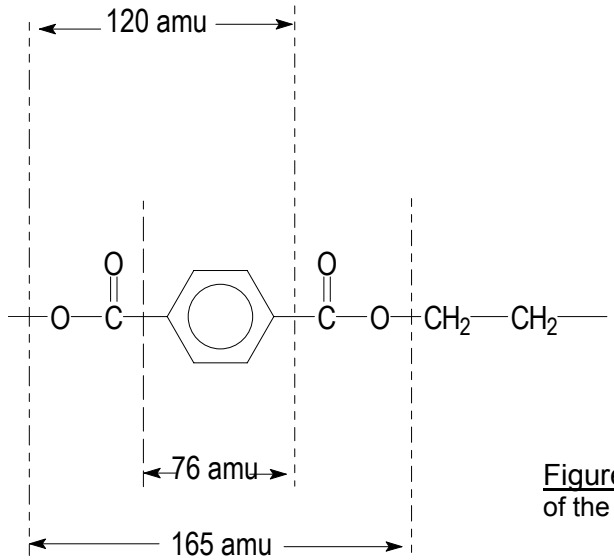

Figure 3.11 Negative ion fragmentation of the PET polymer.

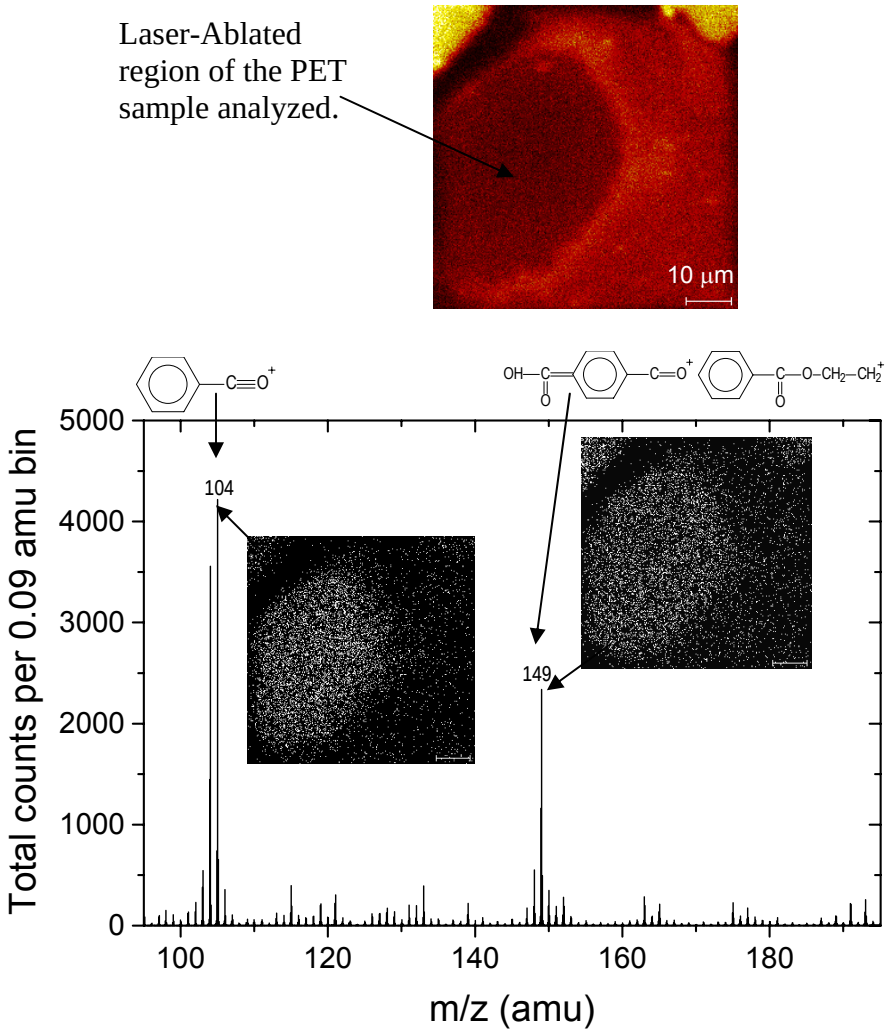

Figure 3.12 Positive PET spectrum collected experimentally from the laser ablated regions.

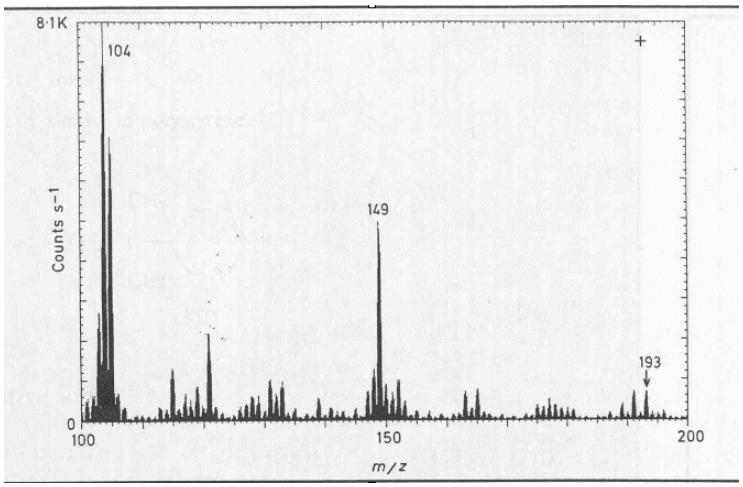

Figure 3.13 The reference for the positive PET spectrum.

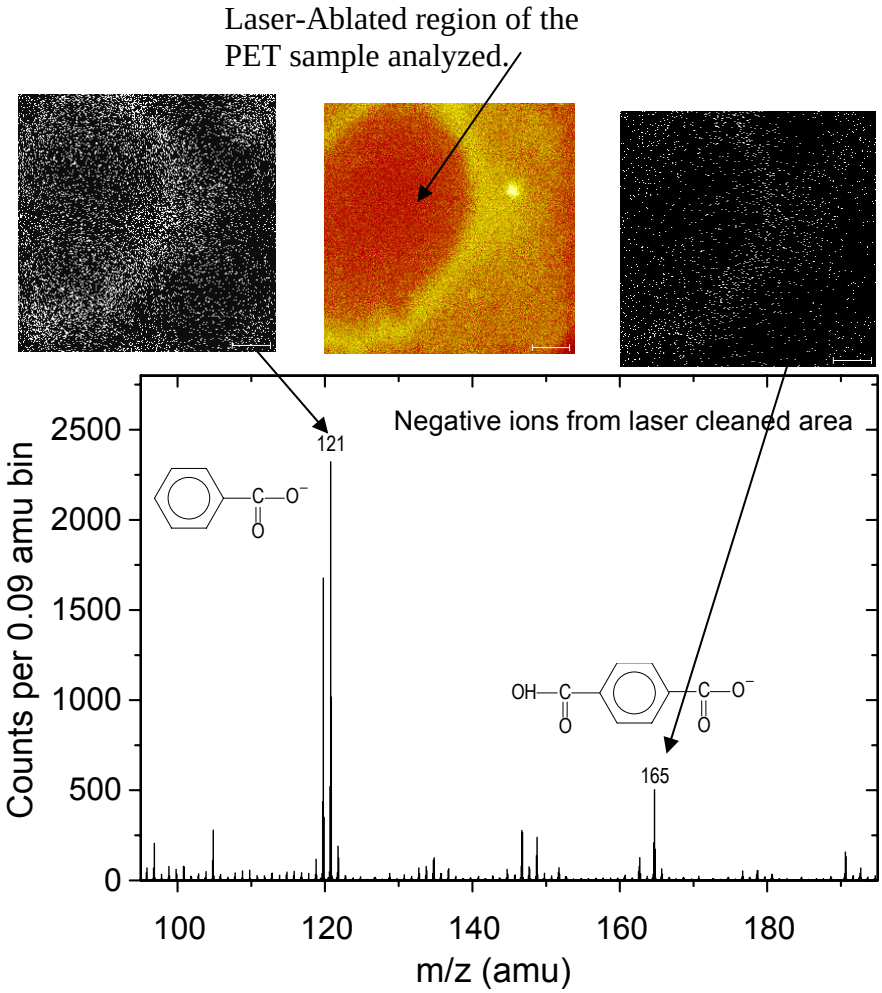

Figure 3.14 Negative PET spectrum collected experimentally from the laser ablated regions.

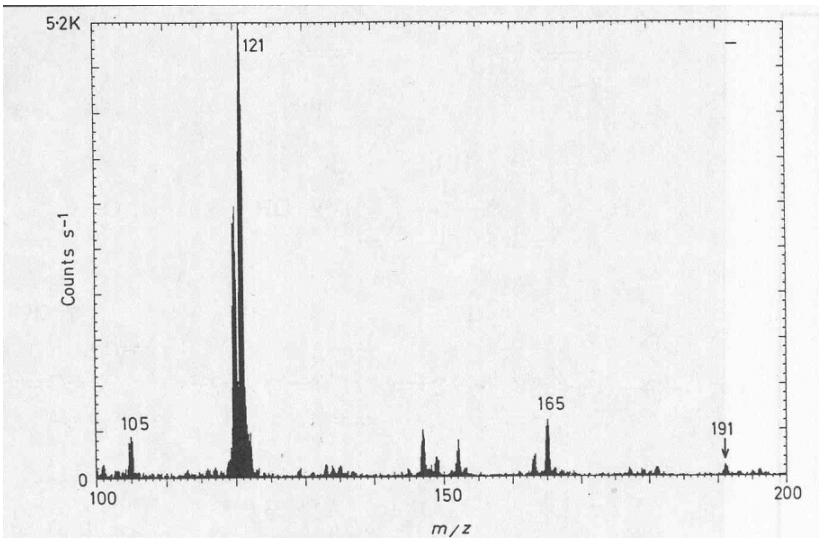

Figure 3.15 The reference for the positive PET spectrum.

Although RTV11 and Intersleek are similar in chemical make-up, in that they both contain the Polydimethylsiloxane (PDMS) polymer, SEM images reveal that the gold removal process via laser ablation in the two polymers is different. It was found that one focused laser pulse removed most of the gold coat in RTV11, whereas Intersleek contained uniform nano-spheres formed by the gold particles left behind after ablation [16].

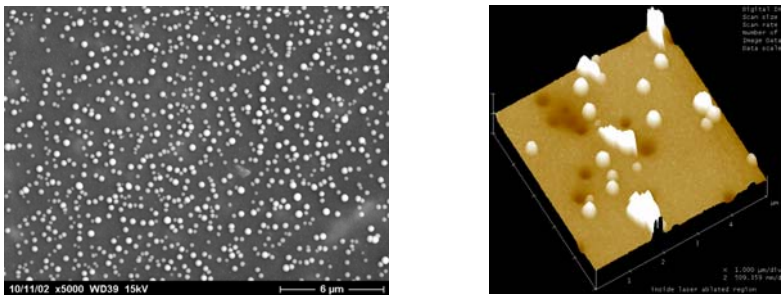

Figure 3.16 Gold particles left behind on the Intersleek surface after one laser shot.

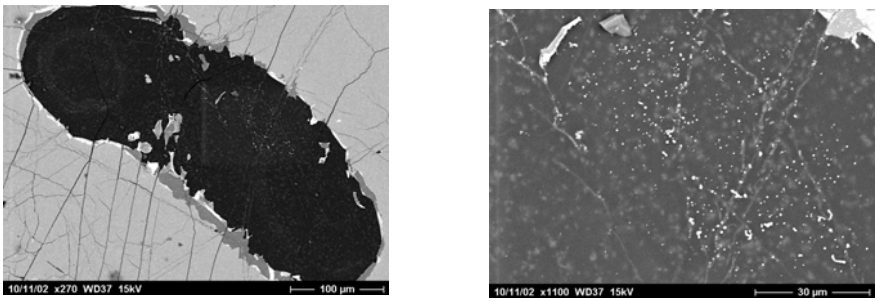

Figure 3.17 Backscattered electron images of laser-irradiated RTV11.

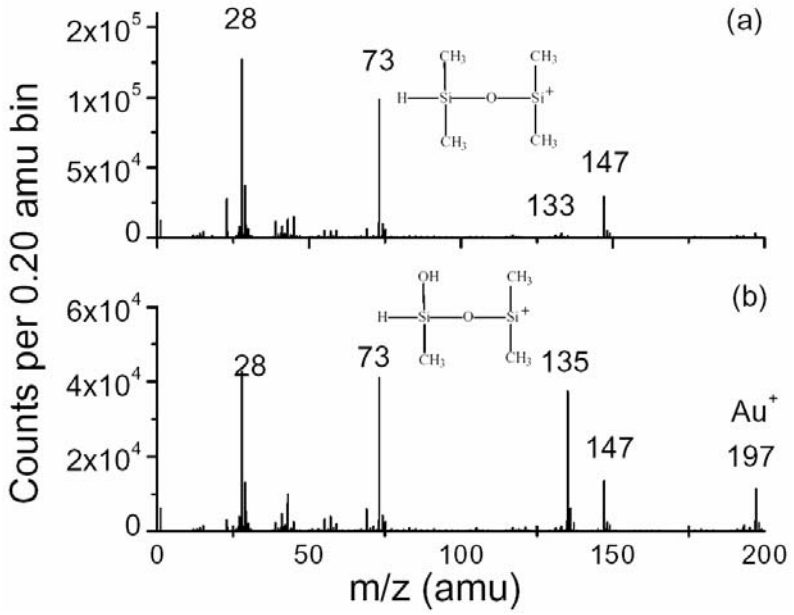

Figure 3.18 ToF-SIMS spectra from laser-ablated Intersleek. Spectrum from region on the sample surface where gold cleaning was complete (a) and data from areas with remaining gold nano-spheres.

Discussions

The removal of thin conducting films by the use of a UV laser source proves to be a promising method for SIMS analysis of thin film coated insulating surfaces. The technique using a 337 nm UV laser does not damage most of the insulating substrates coated with a thin film of gold at reasonable laser fluences. Furthermore, the negligible thickness of the film does not cause fringe fields interfering with the extraction of the secondary ions. The secondary ion extraction from coated insulating surfaces is enhanced considerably with this method as compared with the mesh method. The technique minimizes the effect of surface charging improves the efficiency ion extraction. The ease of collecting quality images and duration of analysis times are comparable to those associated with the flat conducting surfaces [4]. Since the development of this technique, a

considerable number of scientific groups that deal with the development of polymer coatings from government and university laboratories have shown interest in ToF-SIMS analysis of their coating surfaces. The method developed here offers considerable advantage over any other means to analyze a large number of these surfaces within the limited time available in practical applications.

CHAPTER FOUR

LASER INDUCED ENHANCEMENT OF SECONDARY ION DETECTION IN SIMS

The fate and transport of toxic chemicals, as well as toxic metals such as radionuclides in the subsurface soil, have many negative implications particularly when they are involved in groundwater contamination in urban and agricultural areas. For example, during the cold war era, downward migration of radioactive elements as well as many toxic compounds was thought to take thousands of years to migrate appreciably to be a threat to the environment. However, it only took less than 40 years for the groundwater below the Radioactive Waste Management Complex of INEEL (Idaho National Engineering and Environmental Laboratory) to be contaminated by radionuclides such as ^{137}Cs and plutonium [18]. Other organic and inorganic contaminants also mix in the soil. One phenomenon of great interest to scientists is the chemical and physical forms of these contaminants in relation to the subsurface soil minerals and sediments in order to develop remediation methods. Furthermore, it is very important to detect and localize these toxic compounds as early as possible, which means it is necessary to increase the detection sensitivity of these compounds and ions using the smallest amount of toxic material possible. As a part of this research, techniques were developed to increase the detection sensitivity to the radionuclide trace elements absorbed in the subsurface soil.

Leakage of liquid radioactive waste, and waste disposal activities result in contaminant radionuclides such as ^{137}Cs to come in contact with mineral surfaces in the geosphere [19]. A question of great interest is the fate of radiocesium after coming in contact with the mineral surfaces: Will the material be transported or will it remain sequestered due to adsorption to an immobile mineral matrix? Clay minerals possess sheet-like morphology and are hence referred to as phyllosilicates [13]. The adsorption of Cs to phyllosilicates is aided by this morphological characteristic of clay minerals. There are multiple sites within clay mineral where Cs^+ adsorption to the clay can take place. The binding of Cs^+ adsorbed to the surface of the clay, where there are more available sites tends to be weaker and in turn subsequent desorption of the Cs^+ is likely. On the other hand, interlayer sites where Cs^+ adsorption occurs between expandable layers constitute a smaller percentage of adsorption sites. The Cs^+ tends to bind more strongly to these sites however and therefore the transport of the Cs^+ from these sites is expected to be slower [13]. The location of the adsorption sites influences the nature of the radiocesium transport to the environment. As a part of this research, a technique was developed to take advantage of a highly surface-sensitive analytical tool (SIMS) to detect Cs^+ occupying the interlayer adsorption sites in clay minerals.

The technique developed takes advantage of the effect of UV laser irradiation in the redistribution of Cs^+ ions occupying interlayer sites in clay minerals causing these ions to concentrate at the surfaces of mineral particles where an imaging ToF-SIMS instrument can readily detect and localize the

presence of radiocesium. Some of our work on this topic has recently been published in reference [19].

Samples Analyzed

Among samples analyzed were uncontaminated soil samples consisting mainly of unexposed clay minerals (illite, smectite, mixed illite-smectite clays and kaolinite) collected from a 20 foot deep pit located next to a waste disposal area of Radioactive Waste Management Complex (RWMC) at INEEL. These samples were exposed to 1mmol $CsNO_3$ solutions. The RWMC site was used for disposal of waste generated by national defense programs between 1954 and 1970. Also analyzed were kaolinite illite, mixed illite/smectite and montmorillonite clay separates exposed to 1mmol $CsNO_3$ solutions obtained from the Clay Minerals Society, Aurora, CO.

Sample Preparation

Several grains of each of the soil samples and clay separates were placed on individual indium foils approximately 1cm^2 area. Once placed on the foil, glass microscope slides were used to press the grains into the foil to permanently embed the grains in the indium substrate. Subsequently the samples were mounted on the sample holder for placement in the ToF-SIMS instrument for analysis.

Analysis Parameters

The pulsed Ga^+ particle beam analytical probe of the ToF-SIMS instrument was rastered over a $(100\mu m)^2$ area of a mineral particle selected randomly from the particles pressed on the indium substrate. Three different particles were analyzed for a given indium foil. Each pulse of the particle beam was 14 ns in temporal width. A calculated fluence of 2×10^{10} ions $s^{-1}cm^{-2}$ was used to bombard the sample surface for secondary ion emission. Total analysis time was 60 seconds for each sample. Charge compensation via low energy (<20 eV) electron bombardment was used to prevent excessive charging of the sample surface. For every five pulses of primary ion bombardment, one pulse of an electron beam was used.

The imaging nature of the TRIFT I system was utilized to carry out 'Region of Interest' (ROI) analysis of samples. This feature allowed spectrum collection from a user-defined specific area on a previously collected image.

We were interested in whether or not we could promote trace radionuclides to diffuse to the surface under the action of a pulse of UV laser. Such pulse, in principle, can concentrate otherwise dispersed Cs. To examine the modification done by laser irradiation on the sample, pulsed laser irradiation and imaging ToF-SIMS analysis were employed in an alternating fashion. The particle of interest was irradiated by a focused (approximately 30 μm^2) UV pulse in order to locally heat the particle at microscopic scale. The irradiance provided by the laser pulse was estimated to be 1 J cm^{-2}. After irradiation, standard raw data were collected from a 100x100 μm^2 area from which a ROI analysis can be

obtained. A ROI encompassing only the laser-ablated area was retrospectively analyzed with the ToF-SIMS software (WinCadence) to obtain chemical information specific to the ablated area. A similar ROI analysis can also be obtained from the adjacent area not ablated by the laser pulse for comparison purposes. In this fashion, the effect of each laser pulse on the chemical properties of the sample surface could be retrospectively determined by comparing the information collected from the ROI before and after each laser pulse as well as comparing the irradiated vs. unirradiated areas next to each other. In general, it was found that approximately 12 UV pulses produce the maximum concentration of Cs ions. After this dosage, it was found no enhancement was achieved.

Results

As mentioned before, the soil samples collected from the RWMC consisted mainly of illite, smectite and kaolinite. Adsorption of Cs^+ to interlayer sites of these clays depends on the ability of the clay minerals to expand and absorb Cs ions into the lattice structure, which in turn depends on the clay mineral structures. Smectite has a tendency to swell, which means its layers separate. This characteristic of smectite clays allows radionuclides such as Cs^+ to occupy its interlayer sites. Illite and kaolinite both have non-expandable clay structures. Montmorillonite, an expandable phyllosilicate was also among the clay minerals analyzed.

In all instances, the ROI was defined as the laser irradiated area on the sample surface. Often times it is difficult to identify laser-ablated areas on rough surfaces for imaging SIMS, such as soil and clay minerals analyzed here. This difficulty was overcame by imaging, retrospectively, the organic species in the identification of the laser irradiated area [19]. The organic species are removed from surfaces subjected to laser ablation. One such organic molecule, $C_6H_{16}NO$

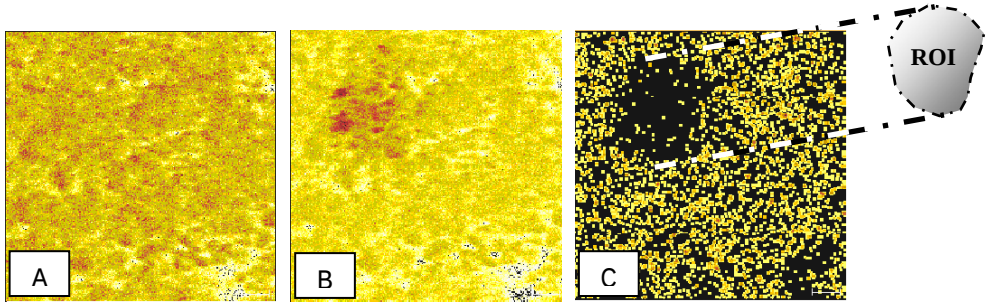

Figure 4.1 Total ion image of the sample: Prior to irradiation (A), post irradiation (B). Image of the $C_6H_{16}NO$ organic molecule post irradiation for ROI defining purposes (C)

(118 amu), was found on the soil samples analyzed here. The selective imaging of this molecule after laser ablation allows for the more accurate identification of the ROI (Figure 4.1).

Although almost all of the 0.1 mmol CsNO3 solution was adsorbed to the soil samples to be analyzed, only very low abundances of Cs+ were evident in the SIMS spectra collected from the samples prior to laser irradiation. This is evident from the fairly homogeneous nature of the total ion images recorded from the soil samples (Figure 4.1A). After the standard photon dose was applied to the surface of this soil sample, another image of the total secondary ion emission was recorded. The laser–ablated area yielded a greater total secondary ion signal after irradiation (Figure 4.1B) even though the $C_6H_{16}NO$ ion signal has decreased (Fig 4.1C). This means while some of the secondary ions such as

$C_6H_{16}NO$ showed a decrease, others such as Cs^+ and K^+ ion yields have shown an increase as a result of laser irradiation. SIMS spectra from this ROI were retrospectively collected to analyze the abundance of the Cs^+ signal prior and post laser irradiation. Whereas no significant signal of Cs^+ was evident prior to laser irradiation of the ROI, post irradiation signal was enhanced by greater than two orders of magnitude.

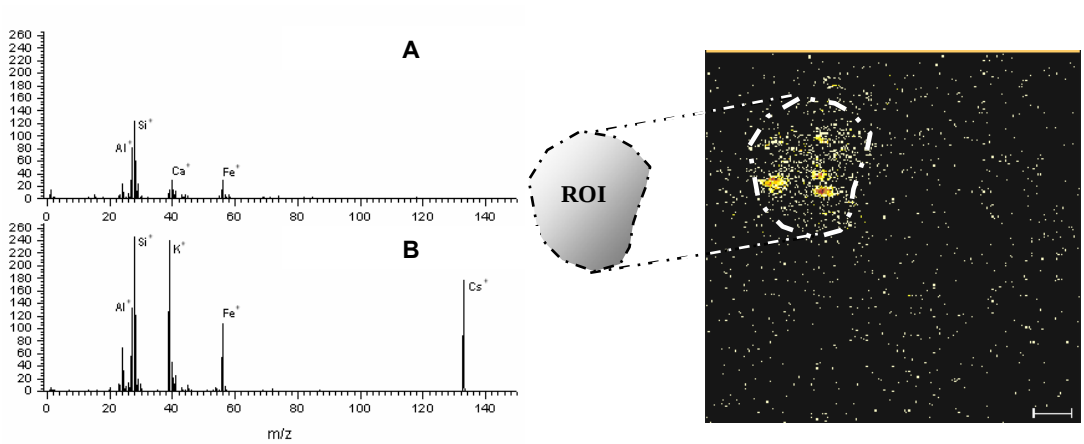

Figure 4.2. Pre (A)- and post (B) laser ablation spectrum collected from ROI. The secondary ion image on the right is representative of the Cs^+ abundance after irradiation.

The Cs+ signal was not the only secondary ion signal enhanced after laser irradiation. The K^+ signal from the laser irradiated ROI was also significantly increased.

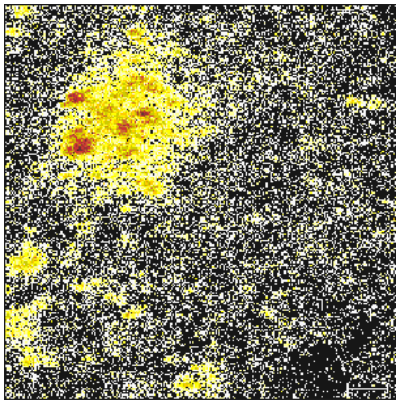

Figure 4.3. Post laser ablation K^+ image collected from the ROI.

It is important to note that the secondary ion signal of K^+, contrary to Cs+ was more homogeneous throughout the laser irradiated ROI. Nearly all of the irradiated area displayed strong enhancement of the K^+ signal. .

In addition to the soil samples, clay separates were also among the samples analyzed. A summary of pre/post laser irradiation enhancement of selected secondary ions is presented below.

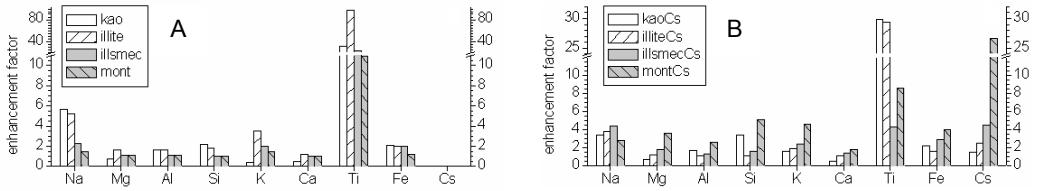

Figure 4.4. Comparison of average enhancement factors for clay separates. (A): Unmodified clay samples and (B): Samples exposed to 1mmol of $CsNO_3$.

The results presented above were obtained from soil samples that were exposed to relatively modest concentrations of $CsNO_3$ (0.1 mmol for soil samples and 1.0 mmol for clay separates). The effect of laser irradiation exposed to greater concentrations (1,10 and 100 mmol) of CsNO3 were also examined. It was found that for increasing concentrations, the soil sample surfaces approached Cs^+ saturation. At high $CsNO_3$ concentrations, the surface is saturated with Cs species, and the laser pulse causes some of the surface Cs to desorp and get replaced by the interlayer Cs ions diffusing to the surface. As a result, non or simply less enhancement of the Cesium signal was observed when pre- and post irradiation spectra were compared.

Possible Mechanism of Cs-redistribution as result of laser illumination

Our view is that Cs is redistributed as a result of the laser pulse and that Cs is concentrated on the surface due to thermodynamical considerations. A possible scenario is that laser heats the surface region and there is a temperature gradient normal to the surface. It is indeed possible that the very top surface layer is cooler than layers below it.

The reason would be that desorption/evaporation of water retained by the clay removes excessive heat from the surface, causing it to cool. This would create a chemical potential gradient for Cs^+ ions to migrate to the surface. Even if there were no chemical gradient near the surface, volatile ions such as Cs^+ would prefer to accumulate on the surface. The surface acts as a reservoir for such ions because it would be difficult for, say, the Cs+ to move to the interior of the clay without displacing other ions in the matrix. This scenario would enrich the surface with highly volatile ions such as Cs^+ and K^+.

Discussions

As mentioned before, the ability to detect and localize toxic compounds in natural soil samples containing only small amounts of these compounds requires increased detection sensitivity. Interlayer sites of phyllosilicate clay minerals comprise a significant portion of the possible Cs adsorptive sites in contaminated soil samples. When a surface sensitive analysis tool, such as an imaging SIMS instrument, is being utilized for the detection purposes of these toxic materials, a

mechanism is needed to redistribute and concentrate to the surface, the Cs+ adsorbed to interlayer sites of the clay minerals. UV laser irradiation proves to be a promising technique of Cs^+ redistribution in soil samples contaminated with trace amounts of Cesium. This technique allows for the early detection of trace amounts of contaminants in soil and clay samples, and therefore introduces an advantage in developing timely remediation methods.

CHAPTER FIVE

OXYGEN EXCHANGE EXPERIMENTS

To gain a thorough understanding of the interaction of contaminants with the geologic subsurface requires the grasp of the mechanisms driving these interactions. Contaminant reactivity on mineral surfaces takes place on the reactive sites of the mineral surface in an aqueous environment. Characterization of the reactive sites on the mineral oxide surfaces is a critical step in developing this understanding. One way of achieving this understanding is to characterize the nature of the oxygen exchange taking place on the mineral surfaces, since O atoms actually define the reactive sites of the mineral surfaces. This can be done using water as the medium of exchange and employing 'heavy' water ($H_2{}^{18}O$ instead $H_2{}^{16}O$) purchased for this purpose. Benefits of understanding the mechanisms of oxygen exchange include: (1) Kinetic stability of oxide surfaces affects a broad range of physical phenomena such as mineral dissolution, sorbtion reactions, stable isotope fractionation and catalyst support degradation. The rate of O-exchange between oxide minerals and the aqueous medium is the most fundamental parameter that enters in understanding the bond-breaking reactions in these multi-step processes. [21] (2) Contaminant interactions with mineral oxide surfaces comprise the principle processes that control the sequestration and transformation. (3) Few methods are available for measuring reaction extend and/or rates and little work has been done to examine

the reactive moieties responsible for adsorbtion and degradation. Finally, (4) Reactive moieties are thought to consist of exposed O atoms in the form of metal/metalloid hydroxyl functional groups such as silanol, aluminol, Fe-OH, or Si-OH groups, which need experimental confirmation.

Our approach is based on our ability of distinguishing between the two Oxygen isotopes ($^{16}O^-$ and $^{18}O^-$), as well as detect accurately the various simple molecules (e.g. SiO_2H^-) involving these isotopes and their combinations such as $SiO^{18}OH^-$. The Oxygen exchange reactions take place in and near the mineral surfaces and understanding the depth of penetration is an important step in understanding the mechanisms of Oxygen exchange. For this reason depth profile experiments were conducted.

Only a limited number of surface analytical techniques exist to enable the characterization of the surface Oxygen species. SIMS methods are very promising, yet achieving chemical specificity to differentiate the many forms of O on the surface is difficult to realize. In general, SIMS spectra offer only non-specific O, OH and metal oxyanions peaks.

A possible method of labeling the reactive sites on these mineral surfaces follows from the fact that different O species undergo O-exchange with water at different rates. Using 'heavy' water, $H_2{}^{18}O$, of different ^{18}O enrichments in the exchange allows us to label the reactive sites on the mineral surfaces. Existing SIMS methods can then be applied to identify these sites.

The main challenge is the depth to which ^{18}O penetrates into a naturally occurring oxide mineral surface, such as SiO_2, due to $^{16}O \Leftrightarrow {}^{18}O$ exchange

reaction. Furthermore, the extent of interaction as well as the mechanism of exchange needed to be understood.

Experimental Procedures

The mineral surfaces selected were natural quartz crystals purchased from rock shops and cut along their $[10\bar{1}0]$ planes. The surfaces were polished to an approximately 50 nm finish. However, in some cases the surface roughness turned out to be much courser than 50 nm, which turned out to be very insightful for interpreting the results. These polished crystal substrates were then baked in atmosphere at 700°C for six hours. This procedure drives any water out of the crystals. The polished surfaces were then sputter-coated with a thin (15 nm) of gold film without keeping them exposed to atmosphere for a prolonged period of time. Subsequent to transferring the substrates to the SIMS instrument, a small portion of this film was removed from the surface of the minerals by using a focused N_2 laser pulse as described above. The laser-ablated areas varied in size in the range of 80-120 μm.

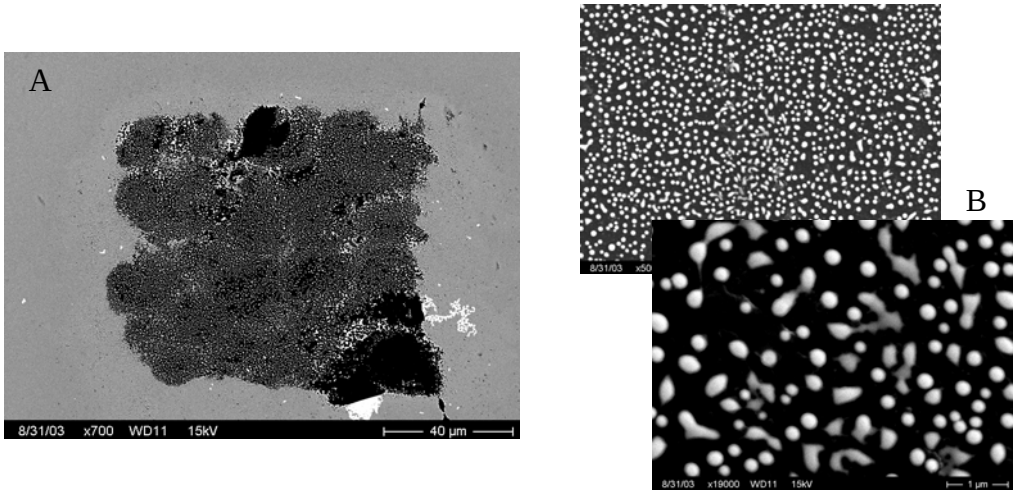

Figure 5.1 A laser-ablated area on gold sputter-coated quartz mineral surface (A). Some gold particles remained even after ablation (B).

The sample was then removed from the ToF-SIMS instrument and allowed to react with water as described in the next paragraph. We have characterized these surfaces by various means of microscopy and spectroscopy techniques first, and later by SIMS experiments and noticed that although most of the gold was removed with laser-ablation, there remained some gold nano-particles on the substrate surface. This is illustrated in Figure 5.1 above.

Some of the laser-cleaned areas of the surface were then exposed to $H_2{}^{16}O$ droplets, while other areas were exposed to ^{18}O-enriched water. The samples were left overnight to react and dry. Finally, depth profiling experiments were carried out on each of these laser cleaned and water deposited areas as well as unexposed areas. Depth profiling was achieved by taking advantage of a continuous Ga+ beam to actively remove material from the surface of the mineral substrate. The surface of the mineral was sputtered in intervals, for a total sputter time of approximately 2000 seconds.

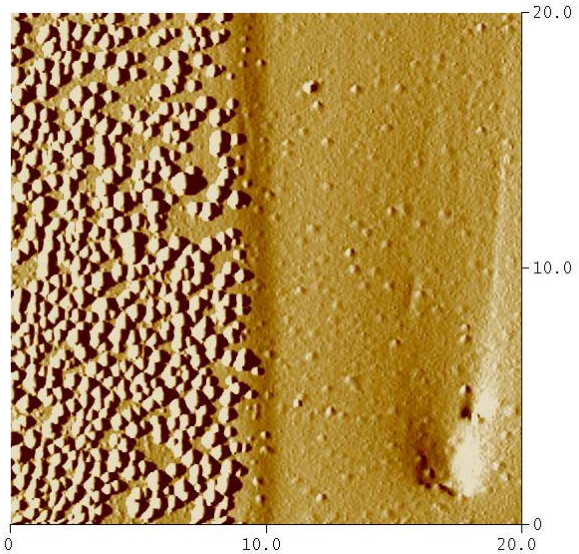

Figure 5.2 The effect of Ga+ sputtering on the quartz mineral surface. The right hand of the AFM image corresponds to the sputtered area.

After each interval of sputtering, a raw spectrum was collected from the laser-cleaned area and retrospectively analyzed by using the region of interest (ROI) function of the WinCadence associated with the sputtered area. In this fashion, concentrations of relevant mass peaks in relation to the total count of secondary ions recorded from the sputtered region were monitored. The depth calibration of the sputter rate was achieved by AFM analysis, and it was found that the Ga^+ sputtering method removed surface material at a rate of 0.7Å/sec. As mentioned above, laser-ablation was not sufficient enough to remove all of the gold used to coat the surface of the quartz substrate. The subsequent particle beam sputter process however did clean the surface of any remaining gold nano-particles. Figure 5.3 below is representative of the concentration of gold relative to total secondary ion count collected from the sputtered area as a function of sputter time.

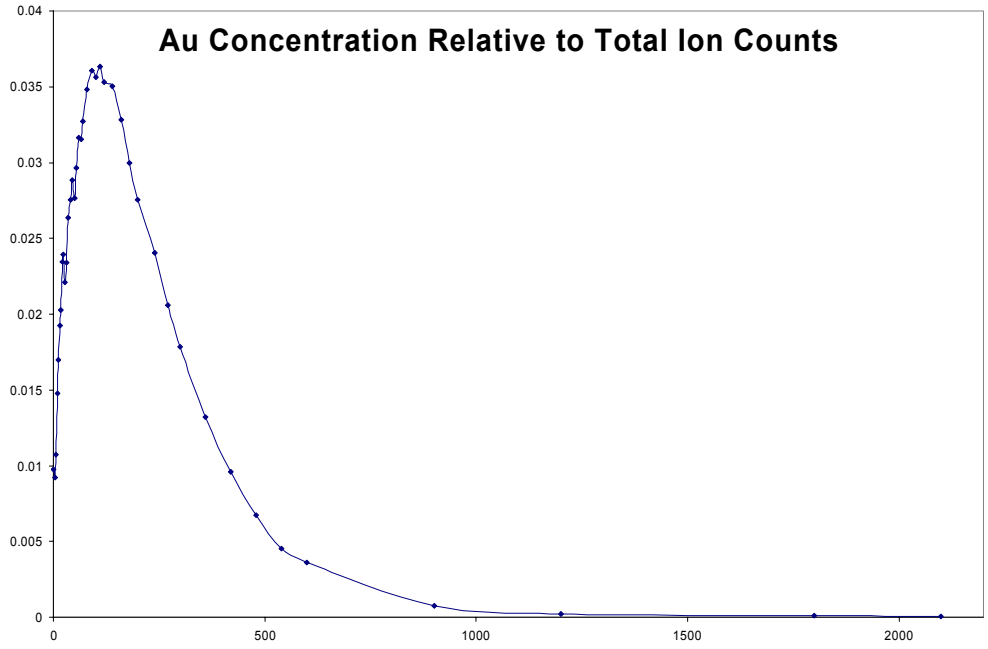

Figure 5.3 Gold concentration from the sputtered area as a function of sputter time.

Depth Profiling & Secondary Ion Distribution

Two different concentrations of, 95% and 47.5% ^{18}O enriched water were investigated. In addition, $H_2{}^{16}O$, deionized water, was also deposited on laser-ablated regions. The concentrations of oxygen moieties were monitored as a function of sputter time or equivalently sputter depth. Concentrations relative to total ions collected from the sputtered region were monitored. Among surfaces investigated were both smooth and rough surfaces alike. A plot representative of the results collected from a smooth surface is presented below in Figure 6.4.

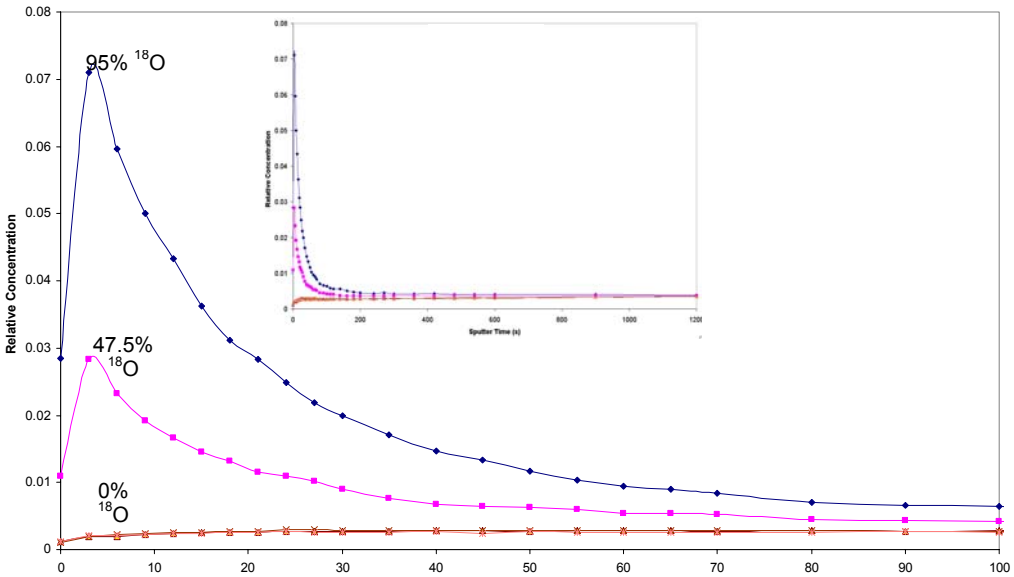

Figure 5.4 Concentration of ^{18}O in the sputtered area as a function of sputter time.

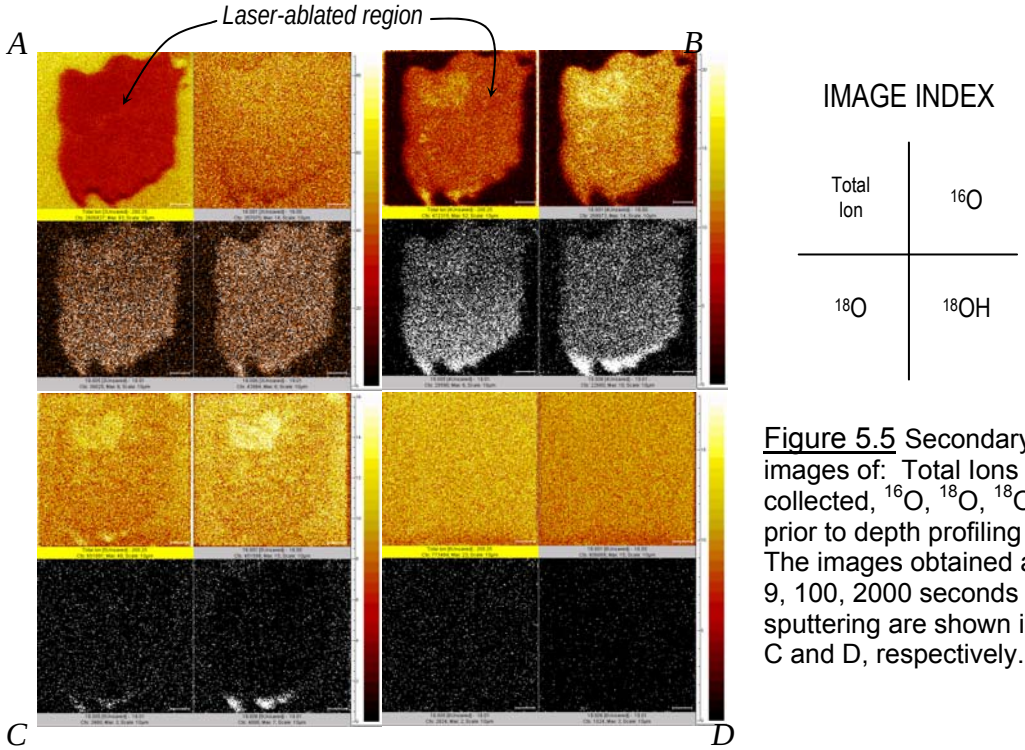

Figure 5.5 Secondary ion images of: Total Ions collected, ^{16}O, ^{18}O, ^{18}O H prior to depth profiling (A). The images obtained after 9, 100, 2000 seconds of sputtering are shown in B, C and D, respectively.

In addition to the smooth surfaces studied, depth profile experiments were carried out with laser-ablated areas on rough surfaces. It was found that ^{18}O deposited on rough surfaces tend to accumulate in specific regions. SEM along with imaging ToF-SIMS chemical images of such a surface is presented below in Figure 5.6.

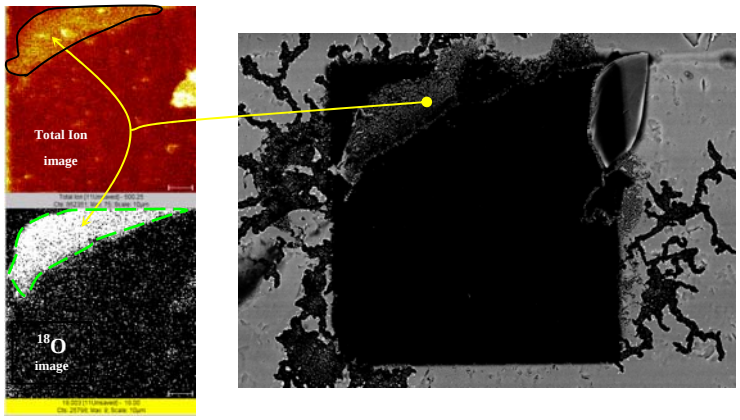

Figure 5.6 SEM and ToF-SIMS images of a rough surface and accumulation of ^{18}O.

Aided by the rough topographical characteristics of this rough surface, most of the ^{18}O deposited on this mineral accumulated in the upper right hand corner of the analyzed (laser-ablated and sputtered) area. Subsequent retrospective analysis of the area showed that the concentration of ^{18}O as a function of sputter depth did not approach zero similar to smooth surfaces analyzed when the whole of the area ablated with the laser pulse was taken into account. When an ROI excluding the region on this rough surface where there was a high accumulation of ^{18}O was considered, the relative concentration of ^{18}O did in fact show behavior very similar to that observed in smooth surfaces. The two ROI's considered are illustrated in the figure below.

A  B

Figure 5.7 ROI's considered with a rough surface. The whole sputtered area (A), and ROI defined by excluding the ^{18}O accumulated area. (B).

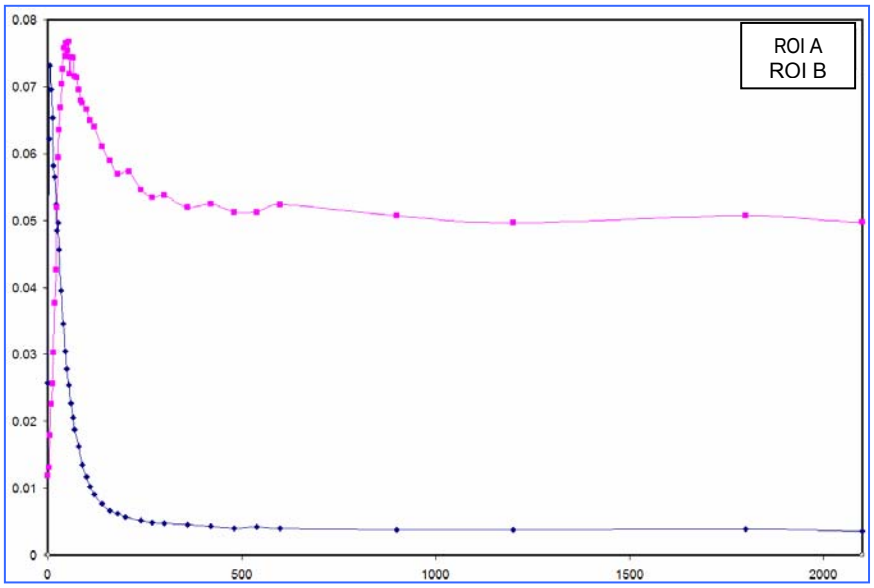

Figure 5.8 Concentration of 18O relative to the total ion counts recorded from the two ROI's.

Possible Mechanism of Exchange

From the depth profiling experiments presented above, it is evident that most of ^{18}O does not penetrate deep into the mineral substrate, but rather resides near the surface. Therefore, it is reasonable to hypothesize that most of the oxygen exchange reactions take place near the surface where ^{18}O molecules of the enriched water deposited on the surface can attach to the unsatisfied Si bonds of the substrate. Furthermore, it is assumed that most of the oxygen exchange is mediated by the high-energy OH groups of the surface [20]. When the ^{18}O enriched water is deposited on the quartz surface, O-H molecules of the enriched water attach themselves to the surface by forming bonds with the surface molecules; ^{18}O form bonds with Si atoms with unsatisfied bonds, and H atoms interact via H-bond with the available ^{16}O. When the substrate is left overnight to dry, most of the evaporated water is $H_2{}^{16}O$, whereas ^{18}O remains attached to Si atoms on the surface, where it can be readily detected by SIMS methods. This hypothesis is illustrated below in Figure 5.9.

Further evidence to support the hypothesis that ^{18}O forms bonds with the surface Si comes when one examines the anion spectra collected from the $H_2{}^{18}O$ deposited regions and these spectra are compared with spectra collected from $H_2{}^{16}O$ deposited regions. It is seen that concentrations of Si and ^{18}O containing molecules desorbed from regions exposed to enriched water are higher than those regions exposed only to ordinary water. Representative spectra are presented below in Figure 5.10.

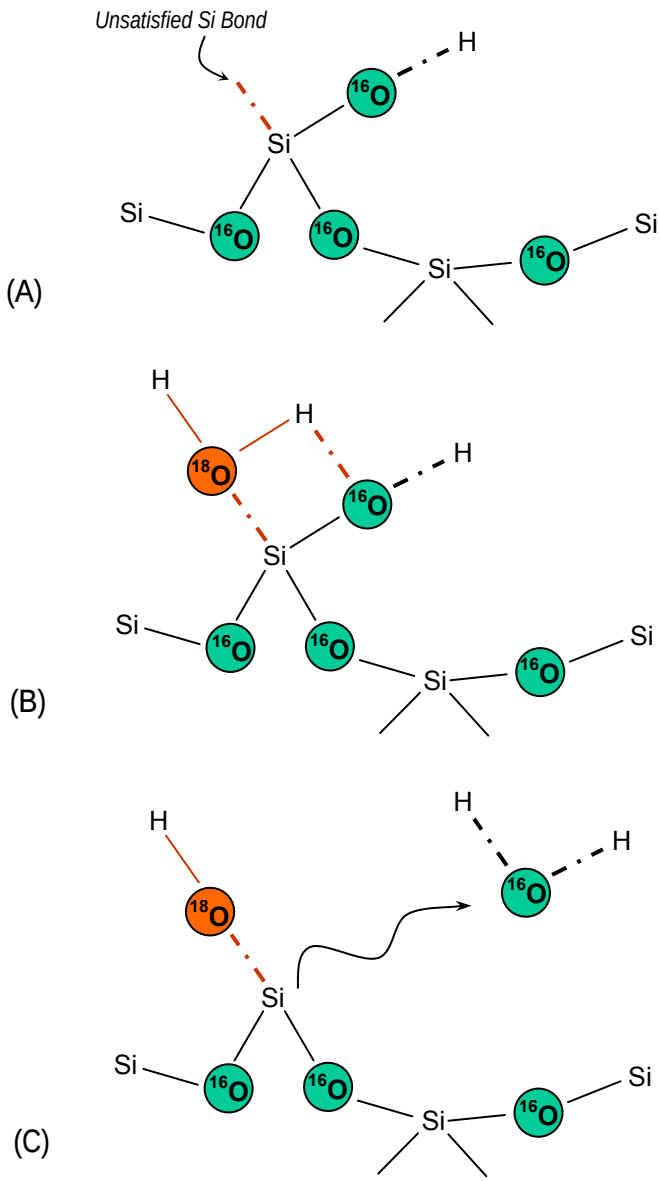

Figure 5.9 Possible mechanism for the ^{16}O-^{18}O exchange. There are unsatisfied Si bonds on the quartz surface before $H2^{18}O$ is deposited on the surface (A). After the enriched water is deposited, ^{18}O form bonds with Si atoms with unsatisfied bonds, and H atoms attach to the available ^{16}O, (B). After the substrate is left overnight to dry, the evaporated water is $H2^{16}O$, and ^{18}O initially deposited, remains behind.

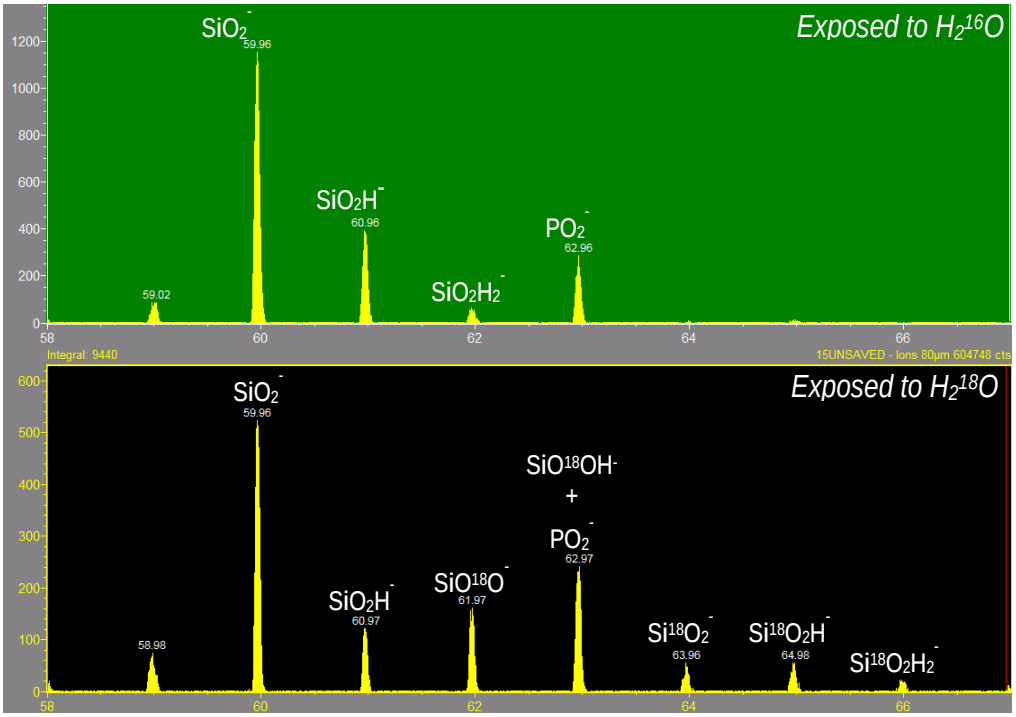

Figure 5.10 Spectra taken from regions that were exposed to the two different types of water. Si + ^{18}O comprised molecules desorbed from regions exposed to $H_2{}^{18}O$ seem to support the idea that bonding between ^{18}O and surface Si atoms occurs, which facilitates the oxygen exchange reactions near the surface.

In conclusion, depth profile experiments point to the evidence that most oxygen exchange reactions occur on the very surface regions of the oxide minerals studied. It is reasonable to hypothesize that the oxygen exchange between the oxide surfaces and water is a thermodynamical equilibrium represented by:

$$H_2{}^{18}O + \text{Quartz Surface} \rightleftharpoons \text{Quartz Surface} + H_2{}^{16}O$$

This equilibrium is energized by the high-energy sites on the surface, and is most likely mediated by the OH groups and by the unsatisfied bonds abundantly present on the mineral surfaces.

CHAPTER SIX

APPLICATIONS of LDMS and LASIMS

MALDI

MALDI (matrix assisted laser desorption and ionization) spectroscopy can be accurately characterized as a special application of LDMS. As explained in earlier chapters, a molecule of interest is dispersed in a matrix to promote desorption and ionization of whole molecular fragments as a result of laser excitation. In what follows, some example spectra to validate the ability of the new platform in carrying out MALDI analysis of a polyethylineglycol molecule at a nominal mass of approximately 5000 amu (PEG 5000) are shown. In this particular case, the MALDI sample was prepared by dissolving 2 mg PEG 5000 material in 0.5 ml aqueous NaCl of concentration 1mg/ml. This dissolved solution was mixed with 1 ml of 40 mM α-cyano-4-hydroxy cinnamic acid (CHCA) in methanol/0.01% trifluroacetic acid 70:30, which serves the matrix function in the final sample.

Figure 6.1 shows the mass spectra associated with this sample, which is used for synthesizing flexible tethers for applications in atomic force microscopy (AFM) and other related fields to attach one molecule to another with a flexible tether. In an AFM application one end of the tether is attached to a protein molecule such as an antibody while the other end is attached to the AFM tip. The AFM side of the tether involves an '*anchoring molecule*' as shown in Figure 6.1.

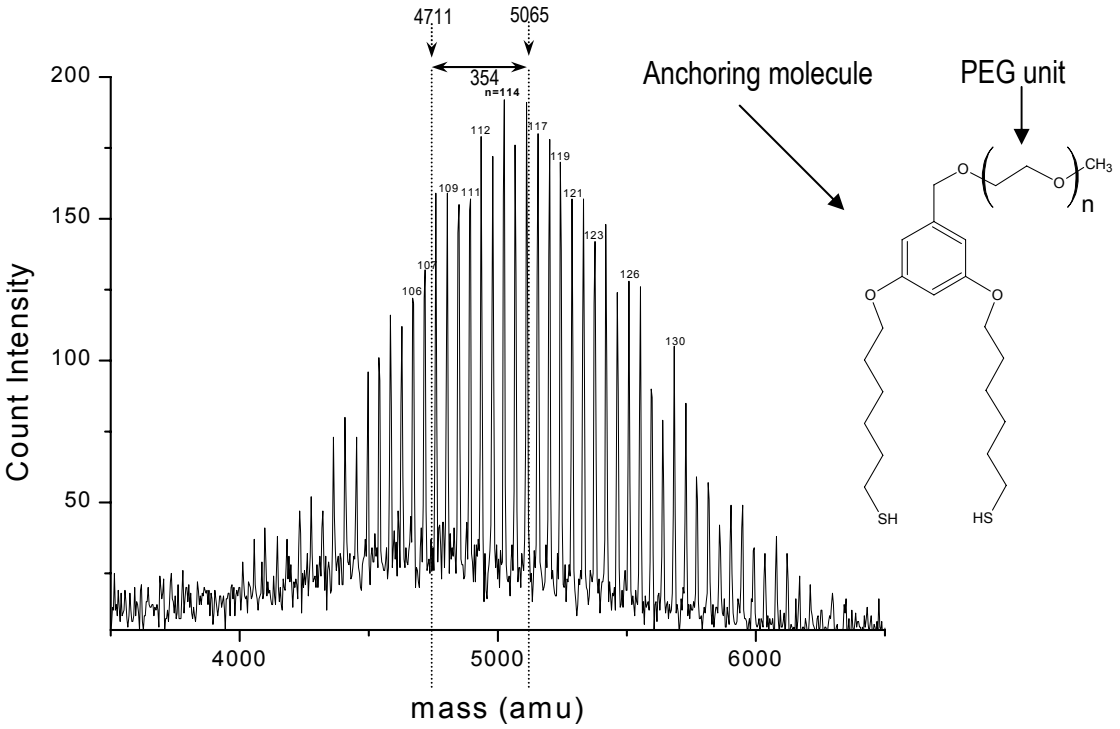

Figure 6.1 MALDI spectra of PEG5000 tether shown above. The series centered around 4711 amu is due to the starting PEG 5000 molecule, while the series shifted by m=354 amu and centered at around 5065 amu is the PEG 5000 tether molecule synthesized to attach to the anchoring molecule (m=254 amu) as marked above.

The anchoring molecule has a nominal mass of 354 amu. Prof. Charlie Spangler and his group synthesize this structure at the Montana State University Chemistry Department. The MALDI experiments were carried out as a part of this research to validate the effectiveness of this synthesis.

With a close look at the spectrum of Figure 6.1, two superimposed PEG-5000 series are observed; the series centered around n=116 (m~5065 amu) is the PEG 5000 tether having a anchoring molecule of 354 amu mass units attached to it, while the background series peaking around n=108 (m~4711 amu) is the starting PEG molecule just before the synthesis, not attached to the anchoring molecule. The detection of the background PEG 5000 series, which

was ‘left over’ from the synthesis demonstrates about 20% of the total PEG5000 molecules were not involved in the tether synthesis.

The fact that the CHCA matrix molecule (shown in Fig. 6.2) is excited by the laser irradiation also results in its desorption, ionization. This molecule is also present in the LDMS spectrum. The nominal mass of this molecule is approximately 189 amu, ultimately giving rise to a reasonably strong peak in the spectrum. The appropriate mass range of the spectrum is presented in Figure 6.2.

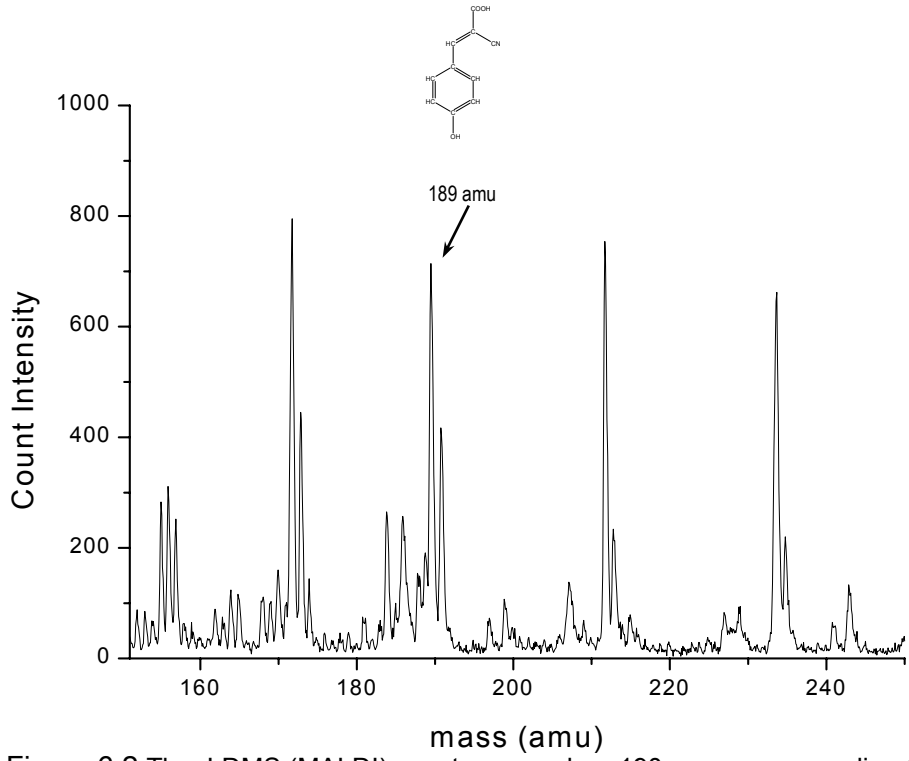

Figure 6.2 The LDMS (MALDI) spectra around m=190 amu corresponding CHCA mass obtained from the PEG 5000 tether mixed into the CHCA matrix as described above. and the molecular structure of CHCA is also shown above.

LASIMS

As it was discussed in some detail in Chapter 1, one of the fundamental motivations behind this work was to test whether or not laser and particle excitation of a surface can couple strongly in the desorbing and ionizing process of secondary ions from surfaces. This idea was tested on a number of samples of varying chemical makeup including simple silicon-wafer surfaces contaminated with the environmental hydrocarbons to large polymeric molecules exceeding mass ranges beyond 5000 amu. The LASIMS experiment involves a short (~4 ns) laser pulse to excite the surface of the sample to just under laser desorption/ionization threshold by means of local heating and/or photochemical processes, while a focused Ga^+ beam that is well synchronized (temporally and spatially) with the laser pulse is used to further energize the sample surface (*LASIMS excitation*) to yield *additional molecular fragments* from that surface. This is a two beam excitation process seeking additional molecular fragments above and beyond the simple superposition SIMS and LDMS spectra obtained by the individual particle and laser excitations, respectively. Existence of such an extra peak or excessive enhancement of existing peaks would mean that there is a strong coupling between the particle and laser excitation mechanisms. However, as suggested by the following examples, we have observed no experimental evidence to support a strong coupling between the two excitation processes. If, however, there exists a rather weak coupling the current statistics associated with our system would not be able detect and resolve this effect. The low repetition rate of the current laser source (≤20 Hz) makes this impossible due

to poor statistics. This however could be improved with a high repetition rate (>1 kHz) UV laser source when such a laser is incorporated into the current LASIMS system.

A large number of systems have been tested. Here we give only three examples. Firstly, Figures 6.3 and 6.4 offers positive ion spectra obtained from a Silicon wafer sample. Two mass ranges included here are: 0-100 amu as well as 100-200 amu. Each mass range are comprised of three mass spectra: An ordinary ToF-SIMS, an LDMS and finally, a LASIMS, which as explained previously consists of a single spectrum obtained by two beam incident on the same are more or less simultaneously. The mass spectra were collected at a 20 Hz repetition rate for all three methods in order to compare the differences and/or similarities.

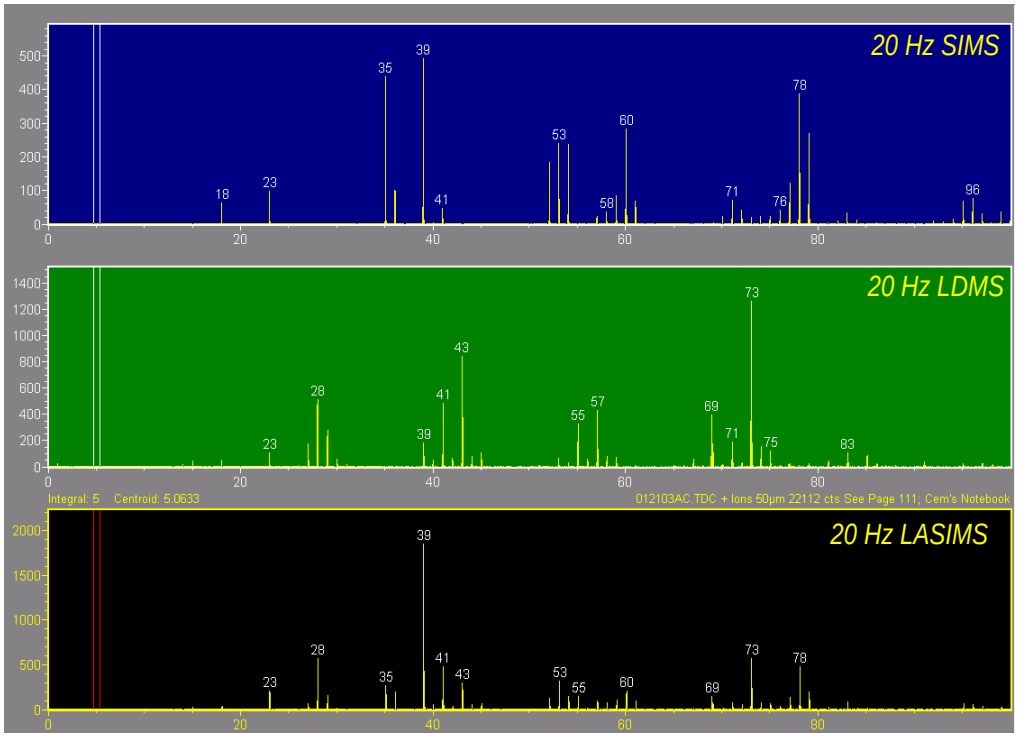

Figure 6.3 Positive ion spectra collected from a Silicon wafer sample utilizing SIMS, LDMS, and LASIMS methods. The spectra correspond to the 0-100 amu mass range. Notice that LASIMS does not show extra peaks but combination of the two above it.

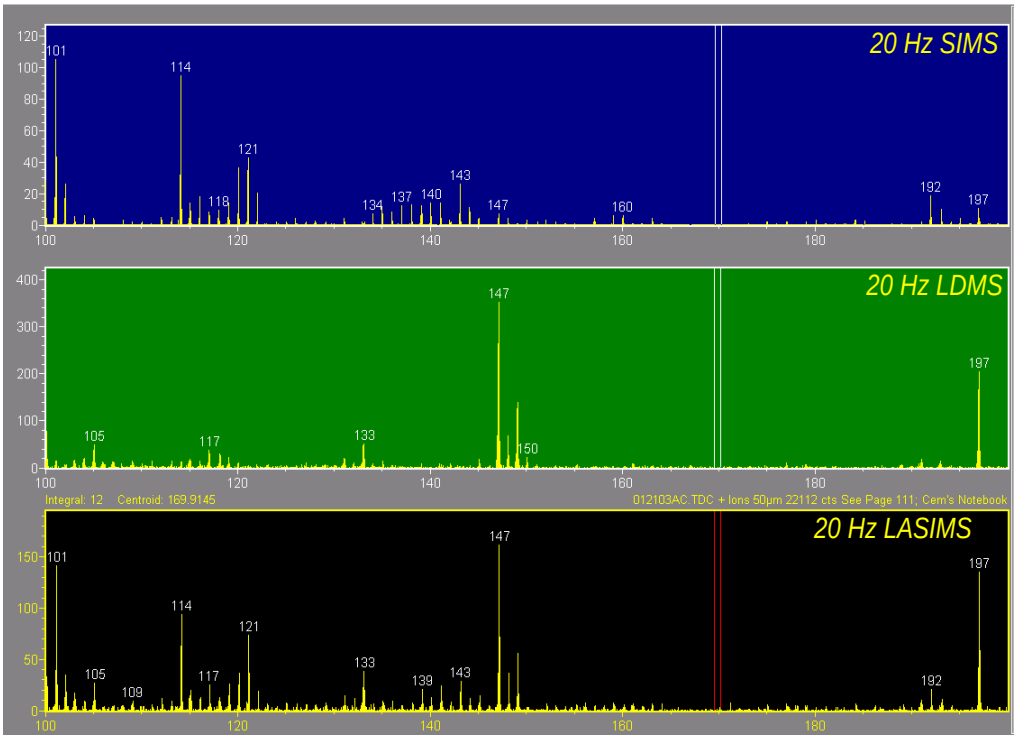

Figure 6.4 Positive ion spectra collected from a Silicon wafer sample utilizing SIMS, LDMS, and LASIMS methods. The spectra correspond to the 0-200 amu mass range. LASIMS simply produces superposition of SIMS and LDMS with no extra features.

For both mass ranges, the observed LASIMS spectrum produces basically the appropriate linear combination of SIMS and LDMS spectra without additional peaks or enhancements. The relative intensities of these peaks are simply a summation of their counterparts obtained utilizing individual SIMS and LDMS methods.

Another example of a LASIMS test is shown in Figure 6.5 below offering positive ion spectra obtained from the same PEG 5000 sample discussed at the beginning of this chapter. The mass ranges of interest is chosen to be 150-295 amu in this case, which contains the 189 amu peak associated with the matrix molecule, CHCA as discussed previously. The figure compares two spectra,

LASIMS and LDMS as described earlier. SIMS shows very little contribution in this region hence it is not included. Again the data acquisition was performed at a 20 Hz repetition rate for both methods in order to compare the differences and/or similarities. As clearly noticeable, the two spectra within the accepted limitations of reproducibility are more or less identical to each other. No excessive enhancement of the matrix molecule at neither 190 amu nor any other fragment are observed, suggesting that laser and particle excitations mechanisms do not couple strongly.

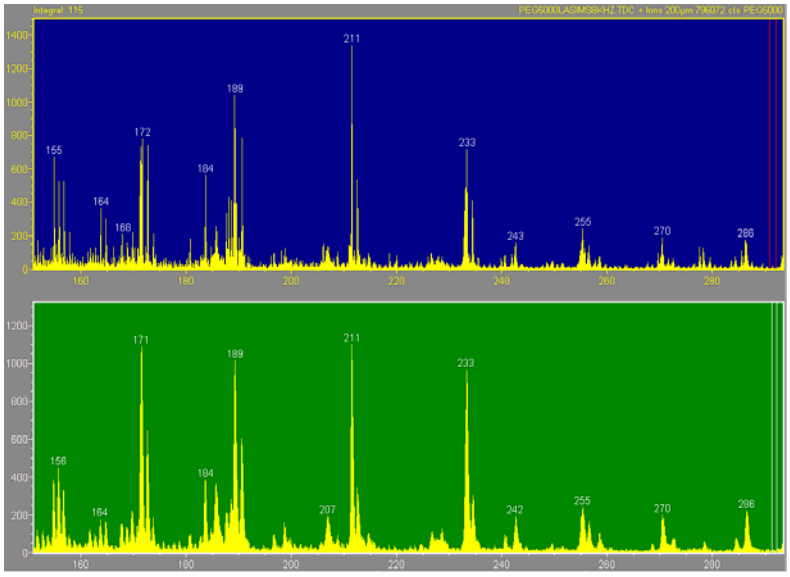

Fig. 6. 5 LASIMS (top) and LDMS (bottom) spectra of PEG5000+CHCA matrix. This experiment targeted the enhancement of the matrix molecule CHCA as a result of LASIMS excitation. However, no excessive enhancement is observed beyond the accepted variations in peak heights and widths.

The final example included here is the LASIMS spectra associated with the 5000 amu region associated with the MALDI excitation process of PEG 5000. Again, no evidence of enhancement beyond the expected variable is observed in

the LASIMS spectra suggesting no coupling between the particle and laser excitation processes.

We have carried out many more similar experiments using organic and biological molecules not included in this thesis with similar conclusions. This result was somewhat surprising for our group because many theoretical considerations as discussed in Chapter 1 implied a possible coupling mechanisms between the two processes. Furthermore, none of the theories studied explicitly acknowledged the lack of coupling between the two processes. Ours is the first experimental evidence suggesting that if any coupling is to be sought it is likely to be a second order effect and might require special samples strongly susceptible to both the particle and laser beam excitations. This subject is still open for further investigation searching for second order effects in the coupling of the two excitation mechanisms by employing high repetition rate laser pulses with improved statistics might result in the sought-after coupling effect.

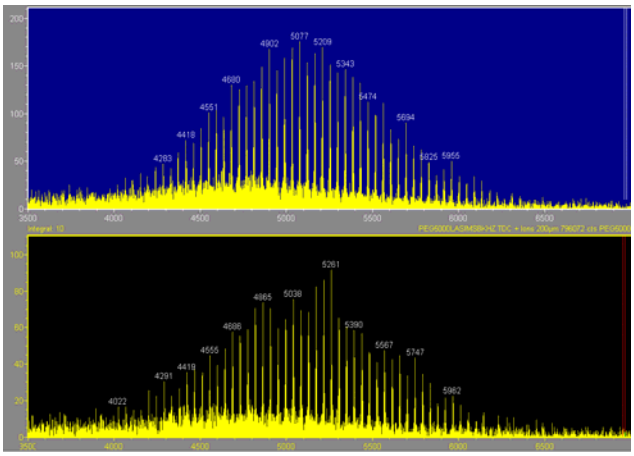

Fig. 6.6 Comparison of MALDI (top) and the LASIMS (bottom) spectra. No discernable differences between the two spectra beyond that of expected variability is observed between the two spectra. No coupling is observed between the particle and laser beam excitation processes.

CHAPTER SEVEN

CONCLUSIONS

In conclusion, a pulsed N_2 laser source was successfully interfaced to an existing ToF-SIMS instrument with sub-nanosecond precision. The interface required tackling hardware and optical issues, plus the development of a LabVIEW based software in order to provide instrument control for the combined system. Additional LabVIEW code was written to address the temporal coincidence requirements associated with the focused particle and photon beams with a sub-nanosecond accuracy. Fulfilling this synchronization requirement ensured valid data acquisition with the customized system. The modifications put in place as a part of this research expanded the functionality of the existing instrumentation to include laser cleaning, modification and analysis of surfaces. Additionally, the combined system offers routine analysis of organic and biological samples by means of LDMS and MALDI methods. The additions delivered with this project expanded the versatility of surface analytical techniques available at the Image and Chemical Analysis Laboratories of Montana State University Physics Department.

Several applications of the new platform have been tested successfully as a part of this research. Firstly, we tested whether or not there is a direct coupling between the particle and laser excitation mechanisms in analyzed surfaces that lead to the desorption and ionization of the secondary ions from them. We

proved experimentally that there is no major coupling between the to excitation mechanisms. The combined system is a very versatile and powerful platform allowing numerous other applications including laser cleaning of thin metallic films coatings on insulating surfaces. This approach allows rapid and practical analysis of very insulating surfaces such as polymers and paints as well as mineral particles. Another advantage of the LASIMS setup is the fact that UV laser irradiation has been shown to cause the redistribution of trace ions such as radionuclides $^{137}Cs^{+}$ hiding in underlying layers of clay minerals in contaminated subsurface soil samples. This redistribution increases the surface concentration of these volatile ions hence improving the detection sensitivity of these radionuclides utilizing ToF-SIMS. This increase in detection sensitivity requires less toxic material to handle in analysis in addition to introducing the advantage of detecting such materials earlier. The system has also been applied in the study of oxygen exchange experiments which proved to confirm the hypothesis that there is exchange of water molecules between the mineral phases mediated by the high energy sites on the mineral surfaces decorated by the hydroxyl moieties.

This research has laid a sound foundation of a very practical and powerful surface analysis platform. A number of scientists from other institutions across the US have shown interest in putting into use our new capabilities. There remains, however, a great deal of room for the improvement of the new system. Expanding the functionality of the new system seems to be the most logical next step. Possible future work includes the interfacing of additional laser sources of

different wavelengths and power. Although we proved that coupling between particle and photon beam excitation mechanisms to be primarily negligible, it is possible that there is a second order effect that exists which couples laser excitation to particle excitation mechanisms for special surfaces. This subject is still open for future investigations.

REFERENCES CITED

[1] http://www.cea.com/tutorial.htm

[2] J.C. Vickerman, A. Brown, N.M. Reed, Secondary Ion Mass Spectroscopy: Principles and Applications: Oxford University Press, 1989.

[3] David S. Selby, *Matrix Assisted Laser Desorption/Ionization Orthogonal Acceleration Time-of-Flight Mass Spectrometry: Development and Characterization of a New Instrument*, PhD thesis, University of New South Wales, 2002.

[4] D.S. Simons, "Laser Microprobe Mass Spectrometry," Proceedings of SIMS IV, pp.158-163, 1983.

[5] M. Karas and F. Hillenkamp, "Laser Desorption Ionization of Proteins with Molecular Masses Exceeding 10000 Daltons." Analytical Chemistry, vol. 60, pp. 2299-2301, 1988.

[6] A. Hachimi, E. Poitevin, G. Krier, "Study Of The Mechanism Of Chromium Cluster Formation By Laser Microprobe Mass-Spectrometry - Correlation With Theoretical Computations," Int. J. Mass Spectrom., vol. 144, pp. 23-45, 1995.

[7] B. Spengler, R. Kaufmann, "Gentle Probe For Tough Molecules - Matrix-Assisted Laser Desorption Mass-Spectrometry," Analusis, vol. 20, pp. 91-101, 1992.

[8] A. Delcorte, X. Vanden Eynde, P. Bertrand, J.C. Vickerman, B.J. Garrison, "Kiloelectronvolt Particle-Induced Emmission and Fragmantation of Polystyrene Molecules Adsorbed on Silver: Insights from Molecular Dynamics," Journal of Physical Chemistry B, vol. 104, pp.2673-2691, 2000.

[9] S.J. Pachuta, R.G. Cooks, "Mechanisms in Molecular SIMS," Chem. Rev, vol. 87, pp.647-669, 1987

[10] A. Overberg, M. Karas, F. Hillenkamp, "Matrix-Assisted Laser Desorption of Large Biomolecules with a TEA CO_2 Laser," Rapid Communications in Mass Spectrometry, vol.5, pp.128-131, 1991.

[11] R.G. Cooks, K.L. Busch, "Matrix Effects, Internal Energies and MS/MS Spectra of Molecular," International Journal of Mass Spectrometry and Ion Processes, vol. 53, pp. 111-124, 1983.

[12] B.W. Schueler, "Microscope Imaging by Time-of-flight Secondary Ion Mass Spectrometry," Microscopy-Microanalysis-Microstructures, vol. 3, pp. 119-139, 1992.

[13] G.J. Leggett and J.C. Vickerman, "Sample Charging During Static SIMS Studies of Polymers," Applied Surface Science, vol. 84, pp.253-266, 1995.

[14] H.W. Werner and A.E. Morgan, "Charging of Insulators by Ion-Bombardment and Its Minimization for Secondary Ion Mass Spectrometry (SIMS) Measurements," Journal of Applied Physics, vol. 47, pp. 1232-1242, 1976.

[15] V. Blestos, D.M. Hercules, J.H. Magill, D. van Leyen, E.Niehuis and A. Benninghoven, "Time-of-Flight Secondary Ion Mass Spectormetry – Detection of Fragments from Thick Polymer Films in the Range m/z ≤ 4500," Analytical Chemistry, vol. 60, pp. 938-944, 1988.

[16] R. Avci, J. Sunner, G. Groenewold, "Laser Cleaning of Gold-Coated Polymers for ToF-SIMS Analysis," Unpublished.

[17] D. Briggs, A. Brown, J.C. Vickerman, Handbook of Static Secondary Ion Mass Spectrometry: John Wiley & Sons 1989.

[18] "Research Needs in Subsurface Science," National Research Council, National Academy Press, Washington, D.C, 2000. Page 30.

[19] G.S. Groenewold, R. Avci, C. Karahan, K. LeFebre, R.V. Fox, M.M. Cortez, A.K. Gianotto, J. Sunner, W.L. Manner, "Characterization of interlayer Cs+ in clay samples using secondary ion mass spectrometry with laser sample modification," Analytical Chemistry, vol. 76, pp. 2893-2901, 2004.

[20] Y.F. Zheng, "On Calculations of Oxygen Isotope Fraction in Minerals," Episodes, vol. 22, pp. 99-106

[21] B.L. Phillips, W.H. Casey, M. Karlsson, "Bonding and Reactivity at Oxide Mineral Surfaces from Model Aqueosus Complexes," Nature, vol. 404, pp. 379-382, 2000.